Ventricular Cardiomyocyte Remodeling in Microgravity Conditions Promotes the Development of Cardiac Alternans through a Calcium-Dependent Mechanism

By

TYMOTEUSZ FRANCISZEK BAK

THESIS

Submitted in partial satisfaction of the requirements for the degree of

MASTER OF SCIENCE

in

Biomedical Engineering

in the

OFFICE OF GRADUATE STUDIES

of the

UNIVERSITY OF CALIFORNIA

DAVIS

Approved:

Eleonora Grandi, Chair

Daisuke Sato

Stefano Morotti

Committee in Charge

2026

1. **Acknowledgements:**

Dr Eleonora Grandi and Dr Daisuke Sato, thank you for being my mentors in this project and pushing me to complete my Master's Thesis. Your mentorship and guidance helped ensure that I was able to succeed in the graduate program and helped me develop as a scientist. In addition, I would like to thank you for your help in preparing this thesis and completing the project.

Dr Stefano Morotti, thank you for agreeing to be on my review committee on very short notice, and for your support during the project. It means a lot that you took the time to help me.

Dr Fazeelat Mazhar, thank you for your continued guidance, patience, and insight over the course of this project. Your mentorship means a lot to me and strongly contributed to my work. I would like to thank you for taking the time to help me.

Dr Amin Forouzandehmehr, Roshni Shetty, Isobella Doherty, and Dr Nathaniel Herrera, thank you for your help, suggestions, advice, and feedback during this project. Your suggestions, and the example you have set with your past work, significantly contributed to my efforts in this project. I would like to thank you for all that you did for me.

Lastly, I would like to thank the remaining members of the Grandi, Sato, and Morotti labs for the guidance and advice they offered me during this project.

2. Abstract:

Microgravity has been associated with increased arrhythmia risk in astronauts, yet the mechanisms underlying this vulnerability remain poorly defined. Experimental evidence suggests that cardiomyocytes under microgravity conditions exhibit changes in ion channel expression and function, mediated by alterations in biochemical signaling and oxidative stress, which could destabilize cardiac action potentials and increase arrhythmia vulnerability. Here we aim to develop a model of cardiomyocyte electrophysiology that integrates experimental results to understand the mechanisms of heightened arrhythmia risk in microgravity conditions.

We adapted a well-established model of the rabbit ventricular myocyte action potential to incorporate experimentally reported microgravity-induced remodeling of L-type Ca^{2+} channels (LTCCs), ryanodine receptors (RyRs), sarco/endoplasmic reticulum Ca^{2+} ATPase (SERCA) pumps, and Na^{+}/K^{+} pumps. We then quantified the effects of microgravity remodeling on cardiac alternans. Using population-based modeling approaches, we assessed the robustness of microgravity-induced effects across a range of cellular phenotypes.

We found that microgravity-induced changes lower the pacing threshold for the onset of action potential (AP) and Ca^{2+} transient alternans, and that these changes arise primarily from increased Ca^{2+} handling instabilities. After isolating the contributions of individual microgravity effects to alternans risk, we found that the remodeling of the LTCC and RyR played a predominant role in mediating the proarrhythmic effects.

Our model contributes to understanding the molecular underpinnings of microgravity-induced arrhythmia and provides a platform to evaluate the efficacy of various interventions on heart health. This can accelerate the development and screening of drug strategies to safeguard astronauts' cardiovascular health, improving the resulting medical outcomes.

3. Table Contents:

4. List of Tables and Figures:

5. Introduction:

Cardiac arrhythmias have been repeatedly documented during spaceflight. In the Skylab program, astronauts experienced multiple instances of premature ventricular contractions (PVCs) (Anzai et al., 2014). In the MIR program, 75 arrhythmias were observed, including a notable case of 14-beat sustained ventricular tachycardia (Anzai et al., 2014). Even short-duration missions posed risks: between 1983 and 1985, 64% (9 of 14) of US space shuttle pilots developed arrhythmias (Anzai et al., 2014). These cases spurred a broad array of studies on the cardiac effects of microgravity to safeguard astronaut health (Sy et al., 2023; Han et al., 2024*a*). The causes of arrhythmia may be attributed to a combination of physiological and environmental factors associated with microgravity and spaceflight, including cardiovascular remodeling (fluid shift, cardiac atrophy, and autonomic imbalance), electrolyte imbalance, oxidative stress, and radiation exposure (Anzai et al., 2014; Sy et al., 2023; Han et al., 2024*a*). Some studies suggest changes in ion channel expression or function in cardiomyocytes under microgravity conditions (Schwoerer et al., 2013; Respress et al., 2014; Yue et al., 2015). These changes can destabilize cardiac action potentials (APs) and Ca^{2+} handling, thereby increasing the arrhythmogenicity associated with the microgravity environment.

As human spaceflight data are limited, various Earth-based models of microgravity have been developed. Head-down bed rest (HDBR) is one such model that was developed using physiological adaptation data from the Soviet MIR program (Pavy-Le Traon et al., 2007). HDBR studies can be safely conducted with human participants and were repeatedly used to study the cardiac effects of cephalic fluid shift. One notable result of these studies is that microgravity exposure tends to reduce the onset heart rate for T-wave alternans (TWA), a symptom of many cardiac pathologies (Grenon et al., 2005; Martín-Yebra et al., 2013, 2015). Although there is no

meaningful change in TWA intensity at resting heart rates (Martín-Yebra et al., 2013, 2015, 2017, 2019), these results reveal a potentially harmful consequence of microgravity exposure.

TWA is a precursor to ventricular tachycardia, ventricular fibrillation, and sudden cardiac death that manifests as beat-to-beat oscillations in the shape of the T-wave on an electrocardiogram (ECG) (Swerdlow et al., 2008; Qu & Weiss, 2023). On a cellular level, this arrhythmia manifests as a beat-to-beat oscillation in action potential duration (APD); however, it is frequently associated with or driven by analogous oscillation in the Ca^{2+} handling of the cell (Mahajan et al., 2008; Swerdlow et al., 2008; Xie et al., 2008; Qu & Weiss, 2023). These oscillations can lead to dangerous arrhythmias through ectopic beats, wavebreak, and reentry (Qu & Weiss, 2023), making the study of TWA essential in cardiac electrophysiology.

Currently, there is a large quantity of data from studies that sought to quantify the single-cell effects of microgravity on ventricular myocytes. Some of these studies induced cephalic fluid shift or cardiac unloading in rodents, while others exposed cultured cells either to true microgravity or analogous environments. Despite the existence of these data and evidence that microgravity exposure increases the risk of cardiac alternans, there have been no mechanistic studies that sought to link microgravity-induced remodeling to alternans risk. This is a major knowledge gap, as such cellular abnormalities are often responsible for tissue- and organ-level dysfunction and pathologies.

Computational modeling can be used to close this knowledge gap and is routinely used in cardiac electrophysiology (Heijman et al., 2016; Trayanova et al., 2024). In this project, we aim to (1) create and validate a new computational model of microgravity-induced remodeling of ventricular cardiomyocytes, (2) test the hypothesis that microgravity-induced remodeling of ventricular cardiomyocytes increases alternans risk, and (3) evaluate the impact of microgravity-

induced molecular changes on cardiomyocyte susceptibility to alternans. Our work integrates experimental observations into a mechanistic framework and provides a novel tool for evaluating antiarrhythmic strategies in astronauts.

6. Methods:

6.1 Baseline Computational Model:

This study uses a model of excitation–contraction coupling in the rabbit ventricular cardiomyocyte developed by Mahajan et al. (2008). This model (Mahajan Model) consists of 26 ordinary differential equations (ODEs) that describe membrane potential dynamics, major transmembrane ionic currents, and intracellular Ca^{2+} cycling. A key strength of this model is its ability to reproduce alternans through two distinct dynamic mechanisms, involving steep APD restitution and intrinsic Ca^{2+} cycling instabilities.

6.2 Parameterization

The effects of microgravity on ventricular cardiomyocytes in various experimental models of microgravity, including hindlimb unloading (HU), heterotopic heart transplant (HHT), and cell-based models, and the corresponding changes to the model parameters are summarized in Table 1. When discrepancies existed among datasets, results from HU studies were prioritized, as this approach represents a more established *in vivo* model of microgravity.

Table 1: Microgravity-induced remodeling summary

	Hindlimb Unloading (HU)		Cell-Based Models	Heterotopic Heart Transplant (HHT)		Parametrized Effect
	Rat	Mouse	Human	Rat	Mouse	Rabbit
SR Ca^{2+} Release Remodeling						
p-RyR (CaMKII)	—	↑[a]	—	↔[b]	—	↑9.4% g_{RyR} ↑9.4% g_{leak}
RyR Gene Expression	—	—	↔[d-f]	—	—	
RyR Protein Expression	—	—	—	↑[b]	—	
Markers of RyR Activity	—	↑[a]	—	↔[b,g]	—	
SR Ca^{2+} Reuptake Remodeling						
p-PLB (CaMKII)	—	↑[a]	—	↓[c]	—	↓2.9% Kmf_{SERCA}
PLB Protein Expression	—	—	—	↑[c,h]	—	
SERCA Gene Expression	—	↔[i]	↔[d-f]	—	—	
SERCA Protein Expression	—	—	—	↔[c,h]	—	

LTCC Remodeling						
LTCC Activation V_m	↓[j,k]	—	—	—	—	↓14.8% g_{LTCC}
Peak LTCC Current	↔[j,k]	—	—	↔[l]	↔[m]	↓5.1mV v_{th}
Na^+/K^+ Pump Remodeling						
Na^+/K^+ Pump Protein Expression	↔[n]	—	—	—	—	↑3.5% g_{NaK}
Na^+/K^+ Pump Activity Assay	↑[o]	—	—	—	—	

RyR: ryanodine receptor, p-RyR: RyR phosphorylation, CaMKII: Ca^{2+}/calmodulin-dependent protein kinase II, PLB: phospholamban, p-PLB: PLB phosphorylation, SERCA: sarco/endoplasmic reticulum Ca^{2+} ATPase, LTCC: L-type Ca^{2+} channel
a. (Respress et al., 2014), b. (Schwoerer et al., 2013), c. (Schwoerer et al., 2008*b*), d. (Han et al., 2024*b*), e. (Mair et al., 2024), f. (Wnorowski et al., 2019), g. (Ibrahim et al., 2012), h. (Ito et al., 2003), i. (Rojo-García et al., 2023), j. (Yue et al., 2015), k. (Halet et al., 1999), l. (Wright et al., 2018), m. (Ritter et al., 2000), n. (Bilichenko et al., 2025), o. (Pamnani et al., 1996)

6.2.1 Ryanodine Receptor Remodeling

Microgravity-induced remodeling is associated with enhanced ryanodine receptor (RyR) activity, as reflected by an increased frequency of Ca^{2+} sparks and spontaneous release events (Ibrahim et al., 2012; Schwoerer et al., 2013; Respress et al., 2014). In the HU model, this effect has been attributed to increased phosphorylation of RyR by Ca^{2+}/calmodulin-dependent protein kinase II (CaMKII) (Respress et al., 2014), whereas HHT studies report increased RyR protein expression (Schwoerer et al., 2013). Microgravity-associated increases in RyR activity were modeled based on hindlimb-unloading data, which attribute enhanced Ca^{2+} spark frequency primarily to CaMKII-dependent RyR phosphorylation. RyR remodeling was parameterized assuming that Ca^{2+} spark rate varies linearly with the fraction of CaMKII-phosphorylated RyR channels, and based on experimental data indicating that fully phosphorylated RyRs exhibit approximately a threefold higher spark rate than non-phosphorylated channels (Soltis & Saucerman, 2010; van Oort et al., 2010; Uchinoumi et al., 2016). From the baseline phosphorylation level of 29% (Soltis & Saucerman, 2010), the reported 25.5% increase in phosphorylation under microgravity conditions from Respress et al. (2014) yielded an estimated

9.4% increase in RyR-mediated Ca^{2+} release. This effect was implemented by scaling the sarcoplasmic reticulum (SR) release flux strength (g_{RyR}, proportional to spark rate) and SR leak strength (g_{leak}) by 9.4%.

6.2.2 SR Ca^{2+} Reuptake Remodeling

Microgravity remodeling has been associated with an increased phospholamban (PLB) phosphorylation by CaMKII in the HU model (Respress et al., 2014), but with a reduced PLB phosphorylation in the HHT model (Schwoerer et al., 2008*b*). As discussed, we prioritized HU data and implemented the microgravity-induced changes in the Ca^{2+} affinity of the sarco/endoplasmic reticulum Ca^{2+} ATPase (SERCA) pump (Kmf_{SERCA}) that are expected from enhanced CaMKII signaling. Experimental studies show that maximal PLB phosphorylation reduces Kmf_{SERCA} by 50% compared to the non-phosphorylated state (Odermatt et al., 1996; Soltis & Saucerman, 2010; Tomek et al., 2025). We assumed a baseline PLB phosphorylation level of 3.3% (Soltis & Saucerman, 2010) and a linear relationship between PLB phosphorylation and Kmf_{SERCA}. To apply the reported 75% relative increase in phosphorylation under microgravity conditions from Respress et al. (2014), we implemented a ~2.9% decrease in Kmf_{SERCA} by directly scaling this parameter in the Mahajan Model.

6.2.3 L-type Ca^{2+} Channel Remodeling

In microgravity conditions, L-type Ca^{2+} channel (LTCC) remodeling is primarily characterized by a shift in the activation midpoint ($V_{\alpha 0.5}$) towards more negative membrane potentials (Halet et al., 1999; Yue et al., 2015). However, experimental studies do not consistently report the accompanying increase in peak current typically expected from this shift (Halet et al., 1999; Ritter et al., 2000; Yue et al., 2015; Wright et al., 2018), indicating that the ion channel conductance may be depressed. We modeled the HU findings of Yue et al. (2015),

showing a -4.9mV shift in $V_{\alpha 0.5}$ and no change in peak current. This effect is implemented by varying the g_{LTCC} and v_{th} parameters to obtain the target $V_{\alpha 0.5}$ and peak LTCC current values (see Section 6.4.1 for details). An example analysis is included in Figure 1, with the results for the baseline and microgravity-remodeled LTCC. The overall analysis identified parameter values that give a -4.82mV activation shift with no change in the peak current.

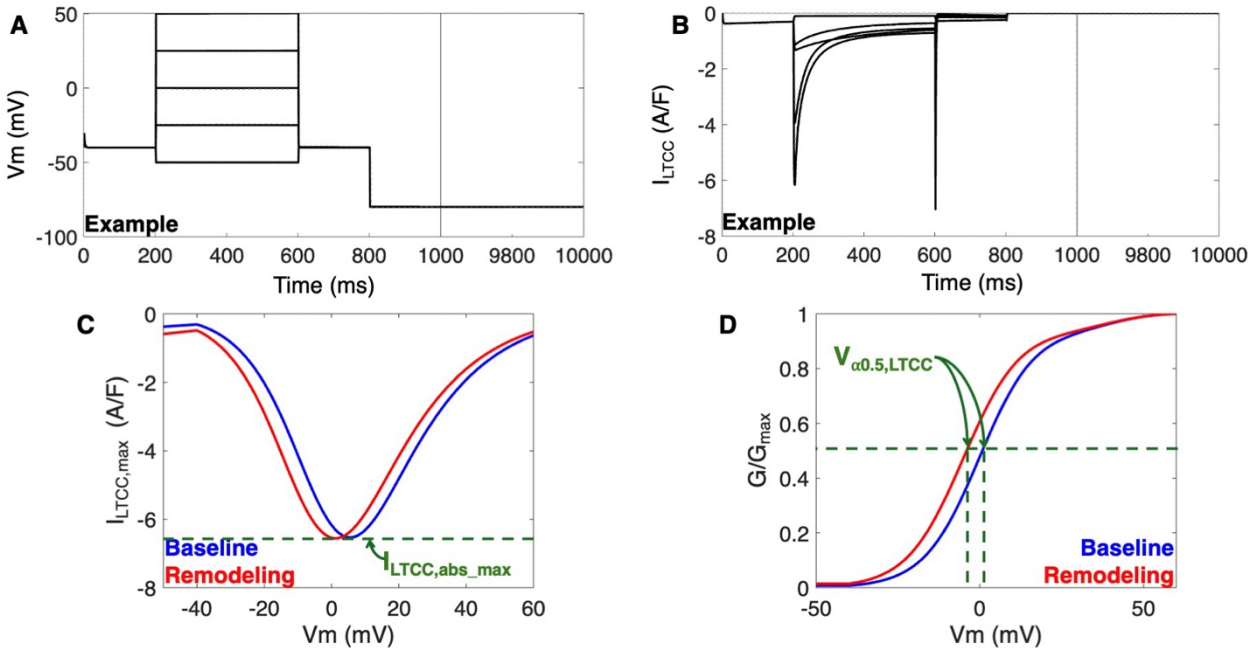

Figure 1: **LTCC parameterization**. The voltage-dependent activation analysis uses a voltage clamp **(A)** to study the LTCC current **(B)**. The maximum LTCC current ($I_{LTCC,max}$) **(C)** and the corresponding LTCC conductance **(D)** are computed for each variable voltage step **(A)**. The target parameters are the absolute maximum LTCC current (dashed line in **C**) and the voltage-dependent activation midpoint (vertical lines in **D**).

6.2.3 Na^+/K^+ Pump Remodeling

The Na^+/K^+ pump is controlled by a ouabain-like inhibitor that is naturally present in the human blood stream (Møller et al., 1990; Mathews et al., 1991). In the HU model, the quantity of this inhibitor is reduced after microgravity simulation, yielding a 3.5% increase in activity when this inhibitor is assayed with canine Na^+/K^+ pumps and a 35% increase in activity when assaying

the native Na^+/K^+ pumps (Pamnani et al., 1996). Given the strong sensitivity of the Mahajan model to changes in Na^+/K^+ pump activity, we implemented the more modest effect and increased the conductance of the Na^+/K^+ pump (g_{NaK}) by 3.5%.

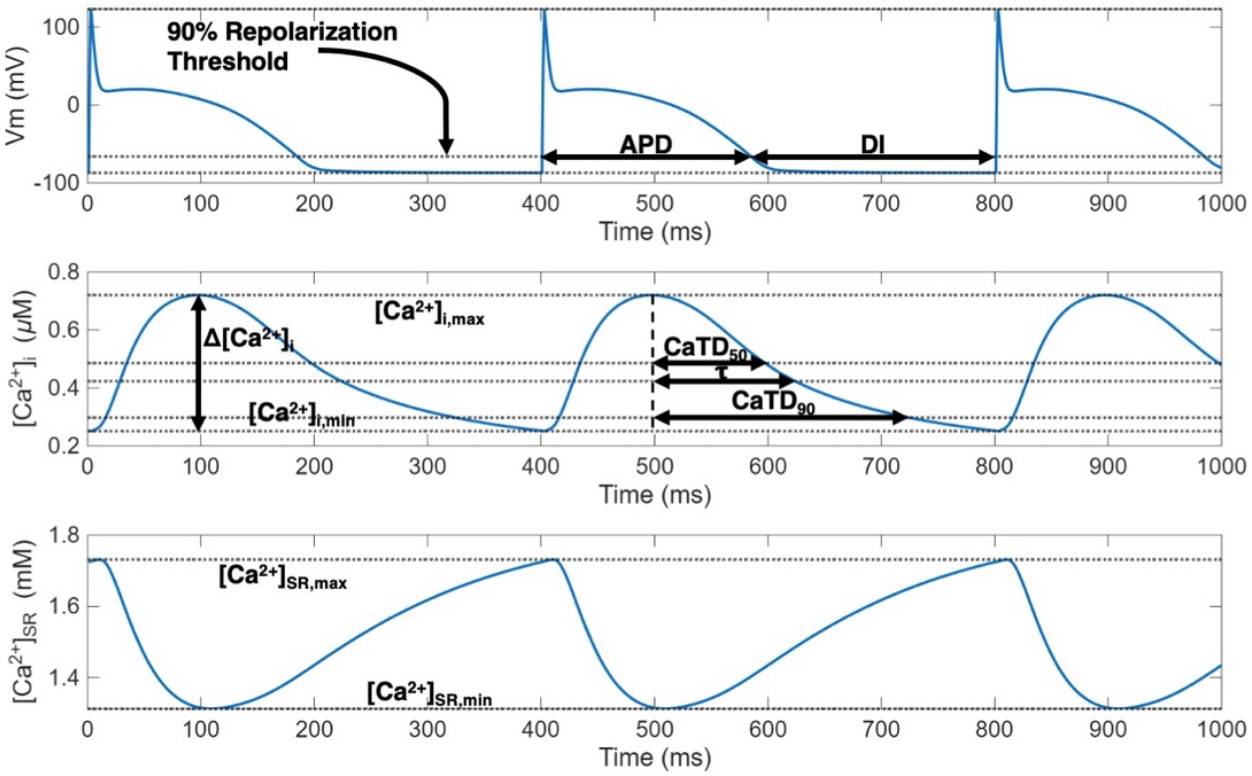

Figure 2: **Biomarker definitions.** The biomarkers are properties of the action potential, Ca^{2+} transient, and SR Ca^{2+} waveforms. APD: action potential duration, DI: diastolic interval, $\Delta[Ca^{2+}]_i$: Ca^{2+} transient amplitude, $[Ca^{2+}]_{i,max}$: peak systolic Ca^{2+} concentration, $[Ca^{2+}]_{i,min}$: end diastolic Ca^{2+} concentration, $CaTD_{50/90}$: time from peak to 50/90% decline in Ca^{2+} transient, τ: time from peak to ~63% decline in Ca^{2+} transient, $[Ca^{2+}]_{SR,max}$: peak non-junctional SR Ca^{2+} load, $[Ca^{2+}]_{SR,min}$: minimum non-junctional SR Ca^{2+} load.

6.3 Biomarker Definitions

The effects of microgravity on ventricular electrophysiology are evaluated using five primary biomarkers (Figure 2). The action potential duration (APD) is defined as the total consecutive time the cell membrane potential is above a 90% repolarization threshold. The peak systolic Ca^{2+} level ($[Ca^{2+}]_{i,max}$) is the maximum cytosolic Ca^{2+} concentration over the course of one basic cycle length (BCL). The end diastolic Ca^{2+} level ($[Ca^{2+}]_{i,min}$) is the cytosolic Ca^{2+} concentration at the end of a BCL. The peak SR Ca^{2+} load ($[Ca^{2+}]_{SR,max}$) is the maximum Ca^{2+} concentration in the non-junctional SR over the course of a BCL. The Ca^{2+} decay time to 50% ($CaTD_{50}$) is the time from the Ca^{2+} transient peak to a 50% decline in the Ca^{2+} transient waveform.

6.4 Simulation Protocols

6.4.1 Parametrization of the LTCC

The Mahajan Model does not explicitly define the values of peak LTCC current or $V_{\alpha 0.5}$; therefore, the target changes in these values are identified by manually analyzing the voltage-dependent activation of the channel using a voltage clamp protocol adapted from Yue et al. (2015). Extracellular and cytoplasmic Na^+ and K^+ ion concentrations were set based on the values reported in the literature (cytoplasmic Na^+: 0mM, extracellular Na^+: 136mM, cytoplasmic K^+: 0mM, extracellular K^+: 0mM) (Halet et al., 1999; Ritter et al., 2000; Mahajan et al., 2008; Schwoerer et al., 2008*a*; Ibrahim et al., 2010; Yue et al., 2015; Acharya et al., 2022). The SR and cytoplasmic Ca^{2+} concentrations were held constant, whereas the subsarcolemmal and junctional Ca^{2+} were allowed to vary because of their close proximity to the LTCC (Bers, 2001). The analysis protocol involved a -40mV prepulse (200ms) to inactivate the fast Na^+ channel (Acharya et al., 2022), a variable test pulse (400ms), a second step to -40mV (200ms), and a recovery

period at -80mV (9200ms) (Figure 1A-B) (Yue et al., 2015). The sequence was repeated ten times for each test potential, and the peak current during the final iteration was measured (Figure 1C). Channel conductance (G) was calculated by normalizing peak current to the driving force for Ca^{2+} at each test potential (Shi et al., 2010). The conductances were further normalized to their maximum value, to obtain the activation plot (Figure 1D).

6.4.2 Computing the Microgravity Effects on Biomarkers

The microgravity and baseline models were paced for 20000 beats at 2.5Hz. Convergence to steady-state is confirmed using APD, $[Ca^{2+}]_{i,max}$, $[Ca^{2+}]_{i,min}$, $[Ca^{2+}]_{SR,max}$, the minimum Ca^{2+} load in the non-junctional SR over one BCL ($[Ca^{2+}]_{SR,min}$), the maximum Na^{+} content in the cell over one BCL ($[Na^{+}]_{i,max}$), the minimum Na^{+} content in the cell over one BCL ($[Na^{+}]_{i,min}$), and $CaTD_{50}$. The biomarkers of interest (see Section 6.3) were extracted at steady-state for both the control and microgravity models and used to estimate their percent changes for microgravity conditions relative to the control.

6.4.3 Population of Models Analysis for Biomarker Effects

To correlate changes in biomarkers to the changes in the microgravity model parameters we used a population of models technique (Morotti et al., 2017; Morotti & Grandi, 2024). A population of 1000 model variations was generated by perturbing 15 baseline model parameters (Table 2) along log-normal distributions (Figure 3A). The standard deviation for this distribution was 10% for non-zero parameters and 1mV for v_{th}. Each individual in the population was paced for 4000 beats at 2.5Hz. An established partial least squares algorithm was used to compute the correlation coefficients that link model perturbations and biomarkers (Morotti et al., 2017, 2021*b*; Ding et al., 2022; Morotti & Grandi, 2024). Statistical significance was evaluated using

the MATLAB fitlm() tool (MathWorks, Natick, Mass), and correlations with $p<0.05$ were considered statistically significant.

Table 2: Population of models analysis input parameters

Parameter	Interpretation
g_{RyR}	SR Release Flux Strength
u	SR Release Slope (Junctional SR Ca^{2+} > 1.5mM)
$J_{up,max}$	Maximum Reuptake Flux
Kmf_{SERCA}	SERCA Affinity for Ca^{2+}
g_{LTCC}	LTCC Flux Strength
V_{th}	LTCC Markov Model Parameter
$g_{to,s}$	Transient Outward K^+ Current Conductance (Slow Component)
$g_{to,f}$	Transient Outward K^+ Current Conductance (Fast Component)
g_{NaCa}	Na^+/Ca^{2+} Exchange Flux Strength
g_{Ks}	Delayed Rectifier K^+ Current Conductance (Slow Component)
g_{Kr}	Delayed Rectifier K^+ Current Conductance (Rapid Component)
g_{Na}	Fast Na^+ Current Conductance
g_{K1}	Inward Rectifier K^+ Current Conductance
g_{NaK}	Na^+/K^+ Pump Current Conductance
g_{leak}	SR Leak Strength

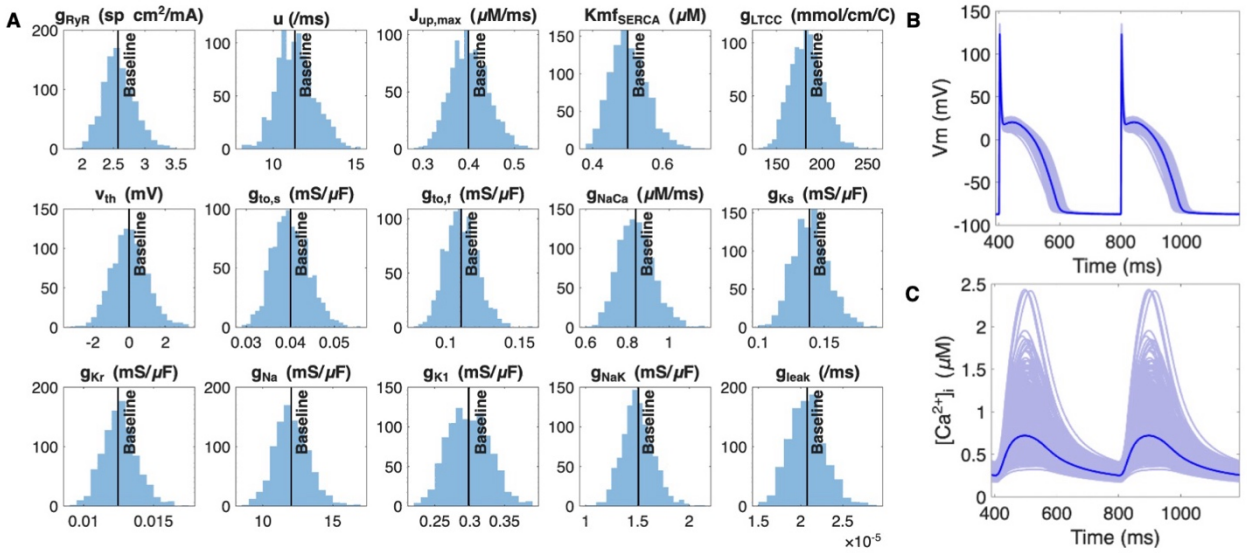

Figure 3: **Population of models**. The input parameters are normally distributed **(A)** and produce variations in the action potential and Ca^{2+} transient waveforms **(B-C)**.

The AP and Ca^{2+} transient waveforms (Figure 3B-C) for each model variant exhibited physiological behavior. The conditions for physiological behavior were defined following examples from Morotti et al. (2021*a*), Morotti et al. (2021*b*), and Ding et al. (2022). In accordance with these conditions, the resting membrane potential was below -85 mV, the AP upstroke was above 0 mV, and the APD was no longer than the basic cycle length (BCL<400ms). In addition, the time to peak (TTP) of the Ca^{2+} transient was no longer than half of the BCL (TTP<200ms).

6.4.4 Perturbation Analysis for Biomarker Effects

To tease out the causal mechanisms linking microgravity to the observed electrophysiological phenotype, we conducted additional simulations in which we separately applied each microgravity effect to the baseline model or restored each of these effects in the microgravity model.

6.4.5 Alternans Threshold Search Algorithm

To determine how microgravity remodeling contributes to alternans initiation, vulnerability to alternans is assessed by estimating the threshold (i.e., longest) BCLs for AP and Ca^{2+} transient alternans in each model variant of the population (see Section 6.4.3). AP alternans is defined as stable beat-to-beat oscillations in APD of at least 5 ms, and Ca^{2+} transient alternans as stable beat-to-beat oscillations in Ca^{2+} transient amplitude ($\Delta[Ca^{2+}]_i$) of at least 10 nM. The threshold for alternans initiation was identified in a predefined range of pacing periods (BCL: 80-600 ms), assuming that every individual exhibits cardiac alternans at fast enough pacing rates (BCL≤80 ms), and none does at slow enough pacing rates (BCL≥600 ms). The protocol evaluates single cell behavior at the boundary pacing periods (BCL=80, 600 ms) and the intermediate pacing period (BCL=340 ms). If alternans appears at 340 ms, then the threshold for

alternans development was inferred to lie in the 340-600 ms BCL range, and BCL=470 ms was tested. Otherwise, the threshold was considered to lie in the 80-340 ms range, and BCL=210 ms was tested. This iterative bisection procedure was continued, progressively narrowing the BCL interval until the alternans threshold was identified. The cell is paced at each tested BCL for 4000 seconds (10000-50000 beats). Convergence to steady-state is confirmed for BCLs that are less than 10 ms from the threshold using the same parameters as in earlier analyses (see Section 6.4.2).

In addition to steady-state convergence, model variants are tested for (1) the absence of alternans at BCL≥80ms, (2) incorrect alternans threshold detection, (3) action potential durations that exceed the BCL, and (4) Ca^{2+} transient recovery of less than 50%. Conditions 3-4 are only applied to the alternans threshold BCL and the nearest BCL to the threshold for which alternans was absent. Twenty-five individuals failed to meet these conditions and after further analysis, seventeen individuals were removed from the study. The remaining eight individuals were returned to the population after resolving the initial threshold identification error. The thresholds for alternans initiation in the population of models are analyzed using the partial least squares technique to determine how they correlate with various aspects of microgravity remodeling (Morotti et al., 2017, 2021*b*; Ding et al., 2022; Morotti & Grandi, 2024).

6.4.6 Bifurcation Diagram Analysis

Bifurcation diagrams are used to describe the frequency dependence of biomarkers and observe the onset of cardiac alternans. The analysis that is used to generate bifurcation diagrams consists of two stages. In the first stage, the cell is paced to steady-state at BCLs from 400 ms to 200 ms, with 10-ms increments. The second stage uses a similar pacing protocol; however, the BCL increment was reduced to 1 ms when the BCL is less than 20 ms from the alternans

threshold in the previous stage. The results were analyzed to confirm that the system converged to a steady-state, in the second stage of this protocol, using the biomarkers listed in Section 6.4.2.

In the first stage of the analysis, the cell was paced for 2000 seconds (5000-6667 beats) for each BCL in the 400-300 ms range and for 4000 seconds (13794-20000 beats) for each BCL in the 290-200ms range. In the second stage, the cell was paced at each BCL for 1000 seconds (2500-5000 beats). The results of the second stage are used in the subsequent data analysis.

6.4.7 APD Restitution Curve Analysis

The APD restitution curves are frequently used to characterize alternans risk (Echebarria & Karma, 2007; Mahajan et al., 2008). In this study they are generated by pacing the cell to steady-state at 2.5 Hz and then pacing for two beats at a variable BCL in the 200-600 ms range. The diastolic interval (DI) before the last beat and the last APD are recorded to create the restitution curve.

6.4.8 Action Potential Clamp Simulation

Action potential clamps are a reliable tool to study Ca^{2+} alternans in the absence of AP alternans (Xie et al., 2008). The action potential recording for this analysis is obtained by modifying the protocol used to obtain the bifurcation diagrams (see Section 6.4.6). The first stage of the analysis remains unchanged; however, the second stage applies the microgravity model threshold from the first stage to the baseline model in the second stage. The AP waveform is extracted for each tested BCL and used to control the membrane potential during the AP clamp simulations. The AP clamp simulations are run for 1000 seconds (2500-5000 beats) at each tested BCL.

6.5 Computational Logistics

The Mahajan Model simulations were solved with the Euler Method using C/C++. The step size was adjusted between 0.01 ms and 0.001 ms to balance the accuracy and speed of the simulations. The data analysis was completed using a combination of Python and MATLAB (MathWorks, Natick, Mass).

The Python, MATLAB, and C/C++ scripts needed to reproduce the simulations and analysis are available on the lab website (https://github.com/drgrandilab).

7. Results

7.1 Microgravity Model Characterization and Validation

The microgravity model exhibits substantial changes in multiple biomarkers, when compared to the baseline model at a 2.5Hz pacing frequency (Figure 4). There is 7% APD prolongation and a 24% $CaTD_{50}$ prolongation. In addition, Ca^{2+} concentrations are depressed with a 22% reduction in $[Ca^{2+}]_{i,max}$, a 5% reduction in $[Ca^{2+}]_{i,min}$, and a 6% reduction in $[Ca^{2+}]_{SR,max}$. These changes were used to validate the model against experimental data, as summarized in Table 3 and Figure 4.

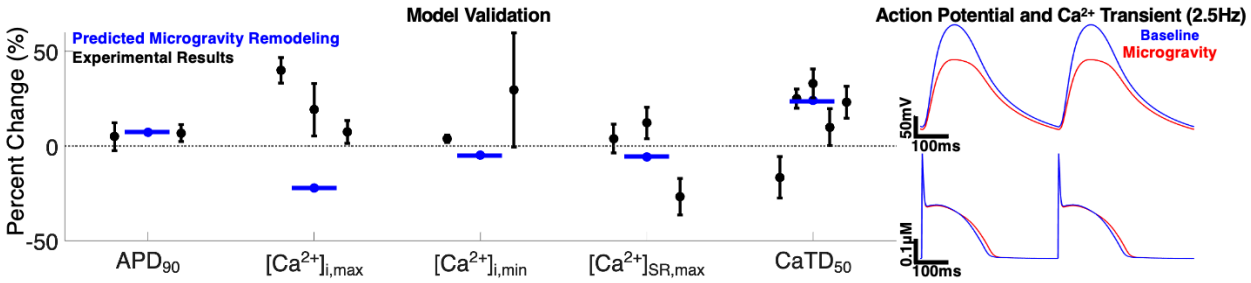

Figure 4: **Model validation**. The percent changes are reported for the biomarkers in HU studies at 2.5Hz pacing (see AP and Ca^{2+} transient traces). These values are compared against the percent change from the microgravity model. No HU data are available for $CaTD_{50}$, requiring the use of data from alternative methods of microgravity remodeling. The error bars correspond to standard error of percent change (United States Census Bureau, n.d.). The data was assumed to be normally distributed for the purposes of generating this plot. (Halet et al., 1999; Ito et al., 2003; Chang et al., 2011; Ibrahim et al., 2012; Moffitt et al., 2013; Respress et al., 2014; Forghani et al., 2025)

Table 3: Microgravity-induced remodeling outcome summary

	Hindlimb Unloading & Head Down Bed Rest (HU/HDBR)			Cell-Based Models		Heterotopic Heart Transplant (HHT)		Reparametrized Mathematical Model
	Rat	Mouse	Human	Mouse	Human	Rat	Mouse	Rabbit
Action Potential Duration Effects								
QT Interval	—	—	$\leftrightarrow^{c\text{-}e}$	—	—	$\uparrow^{f}$	—	↑7.16% APD
QTc Interval	$\leftrightarrow^{a}$	$\leftrightarrow^{b}$	$\leftrightarrow^{c\text{-}d}$	—	—	—	—	
Patch Clamp APD Measurements	—	—	—	—	—	$\uparrow^{g}$	—	
Peak Systolic Calcium Concentration								
$[Ca^{2+}]_{i,max}$	$\uparrow^{h,i}$	—	—	—	—	$\leftrightarrow^{j}$	—	↓22.20% $[Ca^{2+}]_{i,max}$
$\Delta[Ca^{2+}]_i$	—	—	—	—	$\leftrightarrow^{l\text{-}n}$	$\leftrightarrow^{g,j\text{-}k}$	$\uparrow^{o}$	
End Diastolic Calcium Concentration								
$[Ca^{2+}]_{i,min}$	$\leftrightarrow^{h,i}$	—	—	—	—	$\leftrightarrow^{g,j}$	—	↓4.84% $[Ca^{2+}]_{i,min}$
Peak SR Calcium Load								
$[Ca^{2+}]_{SR,max}$	$\leftrightarrow^{h}$	$\leftrightarrow^{b}$	—	—	—	$\downarrow^{g}$	—	↓5.66% $[Ca^{2+}]_{SR,max}$
Calcium Transient Decay Time								
$CaTD_{50}$	—	—	—	—	$\leftrightarrow^{m}$	$\uparrow^{j\text{-}k}$	—	↑24.07% $CaTD_{50}$
τ	—	—	—	—	$\uparrow^{l,n}$	—	—	↑ 19.44% τ
$CaTD_{90}$	—	—	—	—	—	$\leftrightarrow^{g,k}$	—	↑ 7.62 % $CaTD_{90}$

a. (Moffitt et al., 2013), b. (Respress et al., 2014), c. (Sakowski et al., 2011), d. (Solbiati et al., 2020*b*), e. (Solbiati et al., 2020*a*), f. (Schwoerer et al., 2024), g.(Schwoerer et al., 2013), h. (Halet et al., 1999), i. (Chang et al., 2011), j. (Ito et al., 2003), k. (Ibrahim et al., 2012), l. (Han et al., 2024*b*), m. (Forghani et al., 2025), n. (Wnorowski et al., 2019), o. (Ritter et al., 2000)

The microgravity model shows a 7% increase in APD which is well aligned with the hindlimb unloading data, where Respress et al. (2014) and Moffit et al. (2013) show trends toward QTc prolongation (7% and 5%) after 28 days and 10-14 days of HU respectively. However, in HDBR (a human equivalent of HU) QTc intervals on the ECG remain unchanged after microgravity simulation (Sakowski et al., 2011; Solbiati et al., 2020*b*) and the results for QT fail to show a consistent effect (Sakowski et al., 2011; Solbiati et al., 2020*b*, 2020*a*).

APD prolongation is further supported by HHT studies, where microgravity was associated with much larger increases (34% to 182%) than in the HU model (Schwoerer et al., 2013, 2024).

In contrast to the 22% reduction in $[Ca^{2+}]_{i,max}$, the HU studies show an increasing trend. Chang et al. (2011) shows a 7% increasing trend after four weeks of HU, and Halet et al. (1999) show an 18% increase after two weeks of HU. An increase in mean Ca^{2+} content is observed after 1-4 days of *in vitro* microgravity simulation with a random positioning machine (Guarnieri et al., 2021) and no change is observed after 6 days of cell culture in space (Han et al., 2024*b*), further contradicting our results. Although spaceflight studies of cell cultures have shown a small decline in the Ca^{2+} transient amplitude, these changes were not statistically significant (Wnorowski et al., 2019; Han et al., 2024*b*; Forghani et al., 2025). Likewise, the results of most HHT studies fail to support a decline in Ca^{2+} content (Ritter et al., 2000; Ito et al., 2003; Ibrahim et al., 2012; Schwoerer et al., 2013). This limitation of the present model is addressed in the Discussion.

In contrast to the 5% reduction in $[Ca^{2+}]_{i,min}$, the HU studies show an increasing trend. For Chang et al. (2011) this increase is 30%, and for Halet et al. (1999) this increase, which was estimated with a basal calcium quantification, is 4%. This disagreement between our results and

the experimental data represents another limitation which needs to be addressed in future versions of the model. All of the data reported by the HHT studies shows a very mild (<5%) change in $[Ca^{2+}]_{i,min}$, in agreement with the present results (Ito et al., 2003; Schwoerer et al., 2013).

The microgravity model shows a 6% decline in the peak SR Ca^{2+} content which is between the conflicting data points from the HU studies. The HU results of Respress et al. (2014) show a trend towards decline (27%) in SR Ca^{2+} load, whereas Halet et al. (1999) show a trend towards enhancement (12%). A much larger (55%) decline in SR Ca^{2+} content is observed in the HHT study of Schwoerer et al. (2013).

The microgravity model shows a 24% increase in $CaTD_{50}$, which tends to be supported by HHT and cell culture data (Ito et al., 2003; Ibrahim et al., 2012; Forghani et al., 2025). Other Ca^{2+} transient decay times also tend to show marked prolongation in the scientific literature and the microgravity model (Ibrahim et al., 2012; Schwoerer et al., 2013; Wnorowski et al., 2019; Han et al., 2024*b*).

7.2 Microgravity Remodeling Mechanisms at 2.5Hz Pacing

To determine why microgravity remodeling changes specific biomarkers and understand why the microgravity-induced changes agree or disagree with the experimental data, we completed a population of models analysis (Figure 5) and a perturbation analysis (Figures 6-8). The former analysis considers the correlations between model parameters and biomarkers while simulating biological variability (Morotti & Grandi, 2024), and the latter is used to draw definitive conclusions by directly linking causes and effects.

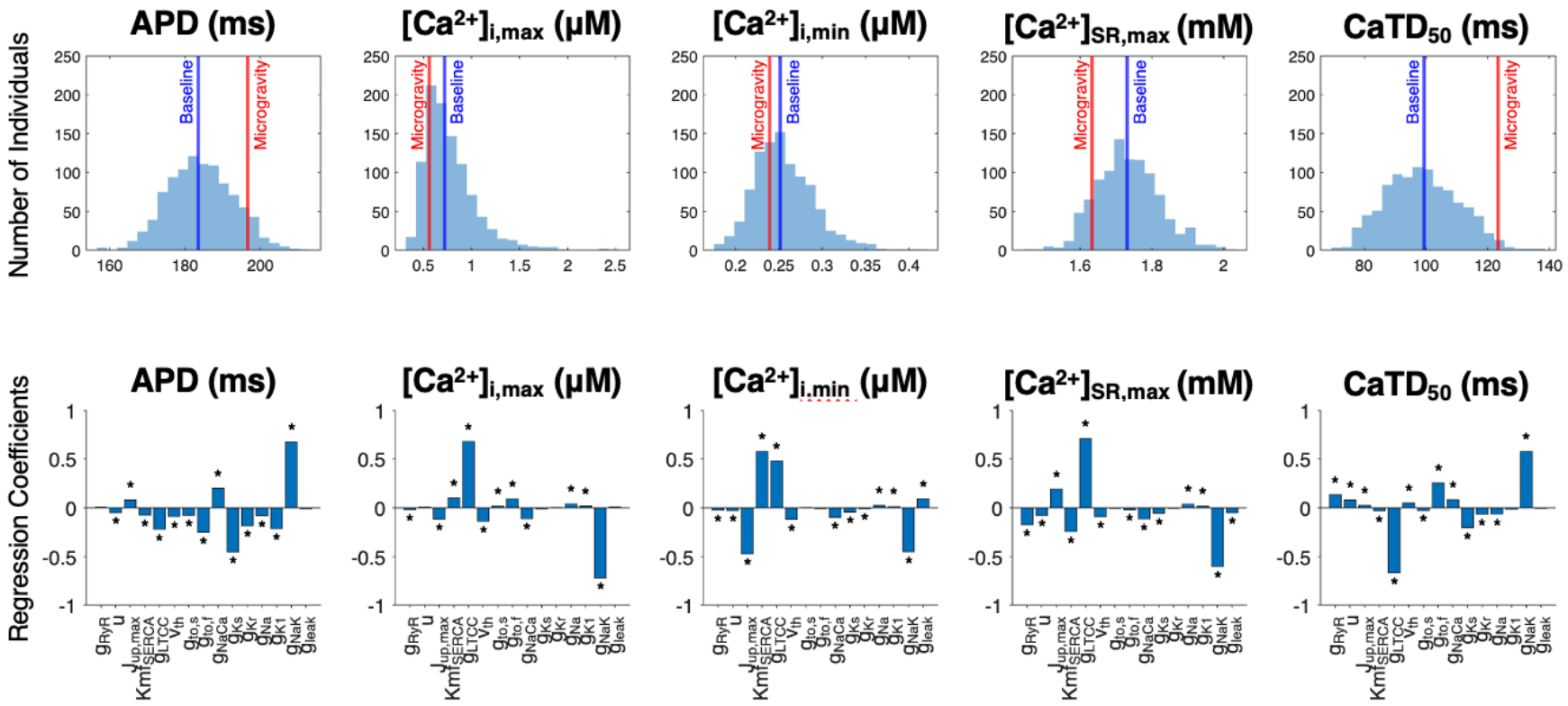

Figure 5: **Population of models analysis results for the primary biomarkers**. The distribution of each biomarker is included (top row) and linked to the model perturbations using an established partial least squares algorithm (bottom row) (Morotti et al., 2017, 2021*b*; Ding et al., 2022; Morotti & Grandi, 2024). These results correspond to a 2.5Hz pacing frequency. *p<0.05

Microgravity-enhanced SR release, leak, and reuptake did not have a strong correlation with any of the biomarkers (Figure 5), with the notable exception of the positive association between Kmf_{SERCA} and $[Ca^{2+}]_{i,min}$. This is important when interpreting the decline in $[Ca^{2+}]_{i,min}$ because lower Kmf_{SERCA} values indicate a greater SERCA affinity for cytosolic Ca^{2+}, and therefore more efficient Ca^{2+} reuptake into the SR. Reducing the LTCC conductance causes a predictable decline in the calcium transient and SR Ca^{2+} load; however, it also produces a $CaTD_{50}$ and APD prolongation (Figure 5). The voltage-dependent activation of the LTCC does not have a strong correlation with the biomarkers (Figure 5). The upregulation of the Na^+/K^+ pump is strongly correlated with APD and $CaTD_{50}$ prolongation and a reduction in cellular Ca^{2+} content (Figure 5).

The correlations presented here provide an overview of how the baseline model changes in response to perturbations in its parameters; however, they ignore the magnitude of the model changes in both the inputs and outputs of the analysis. The perturbation analysis (see Section 6.4.4) overcomes this limitation by revealing the physiological importance of each microgravity-induced effect. The remodeling of g_{RyR} (↑9.4%), g_{leak} (↑9.4%), and Kmf_{SERCA} (↓2.9%) tends to produce small effects on the biomarkers. In contrast, the reduction in g_{LTCC} (↓14.8%) has a profound impact on each biomarker (Figure 6), in-line with the correlations predicted by the population of models. The shift in voltage-dependent activation (↓5.1mV) is significant for all biomarkers except $CaTD_{50}$, shows a meaningful APD prolongation, and increases the Ca^{2+} content of the cell (Figure 7). The remodeling of the Na^+/K^+ pump conductance (↓3.5%) influences the biomarkers as predicted by the population of models (Figure 8); however, this effect tends to be weaker than that of the changes in the LTCC parameters.

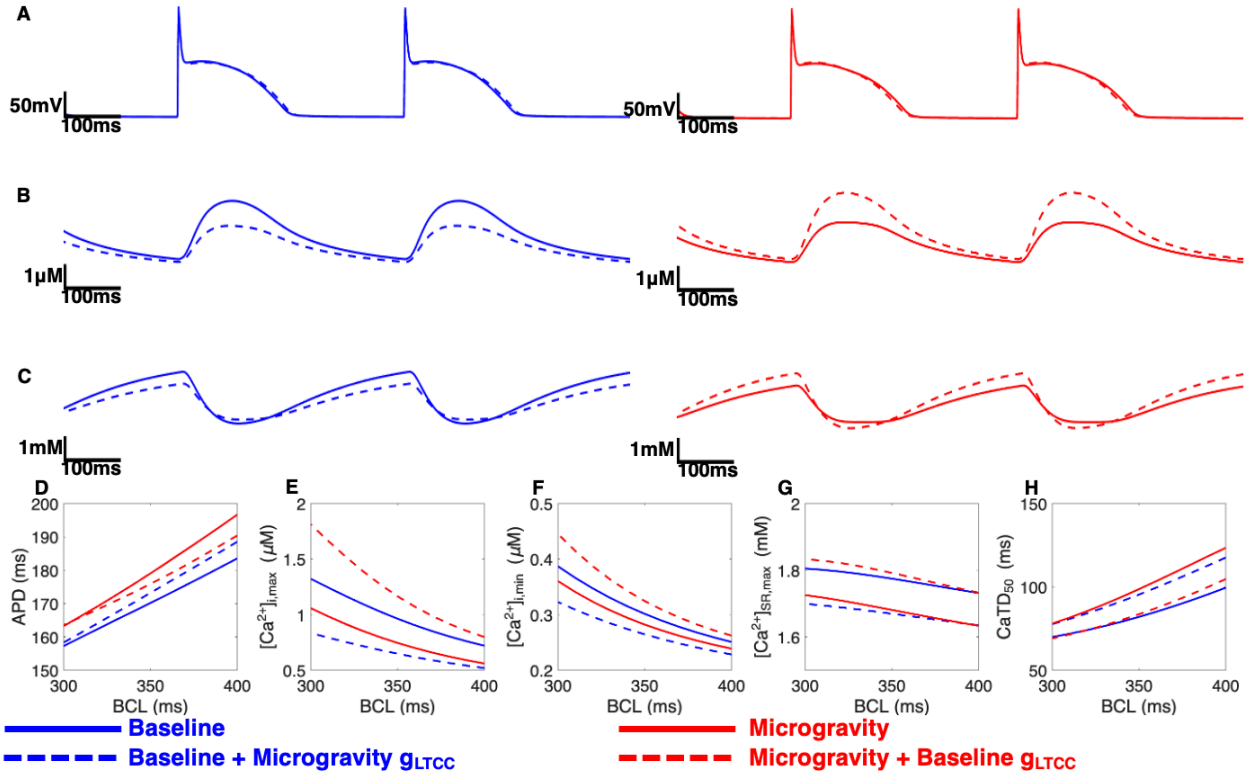

Figure 6: **LTCC conductance downregulation effects**. Action potential **(A)**, Ca^{2+} transient **(B)**, and non-junctional SR Ca^{2+} content **(C)** waveforms are analyzed at 2.5Hz with and without g_{LTCC} downregulation by 14.8%. The key biomarker analysis **(D-H)** shows a significant g_{LTCC} effect over the BCL range of 300-400 ms.

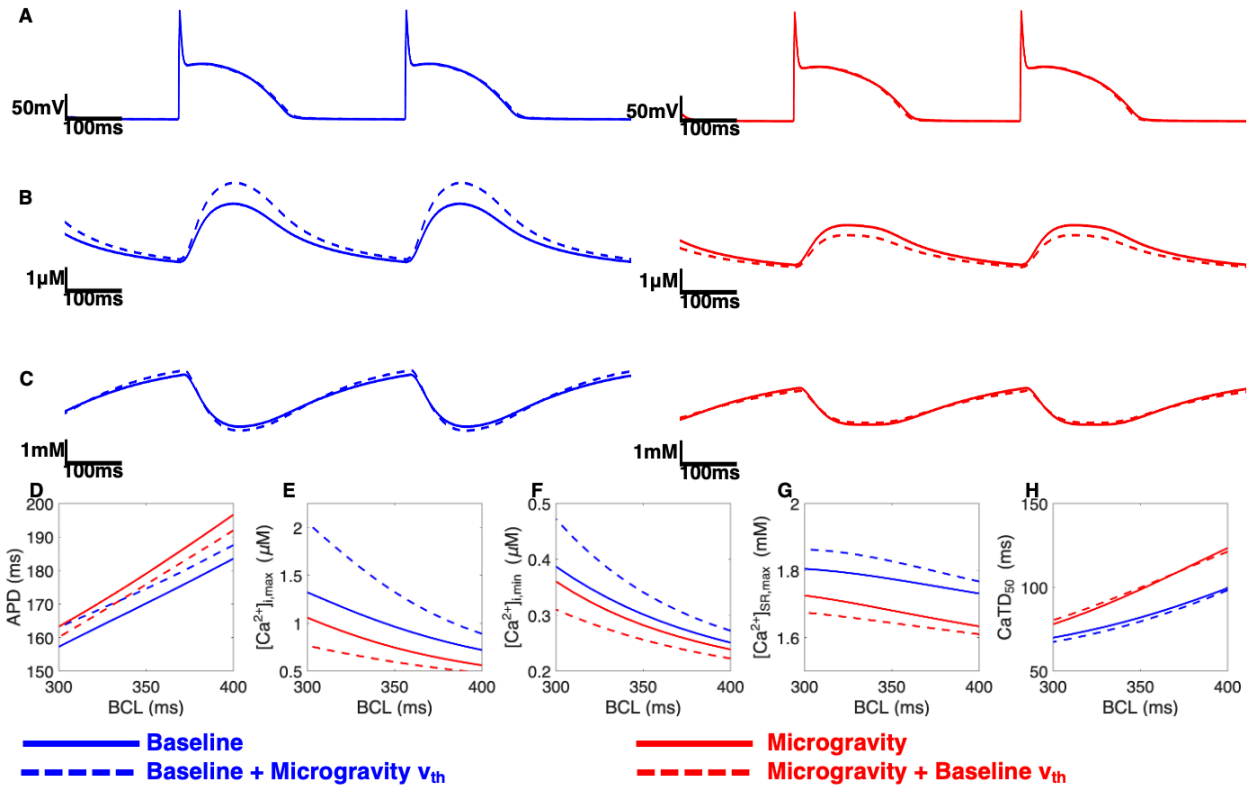

Figure 7: **LTCC activation shift remodeling effects**. Action potential **(A)**, Ca^{2+} transient **(B)**, and non-junctional SR Ca^{2+} content **(C)** waveforms are analyzed at 2.5Hz with and without a v_{th} reduction of -5.1mV. The key biomarker analysis **(D-H)** shows a significant v_{th} effect for all biomarkers except $CaTD_{50}$ over the BCL range of 300-400 ms.

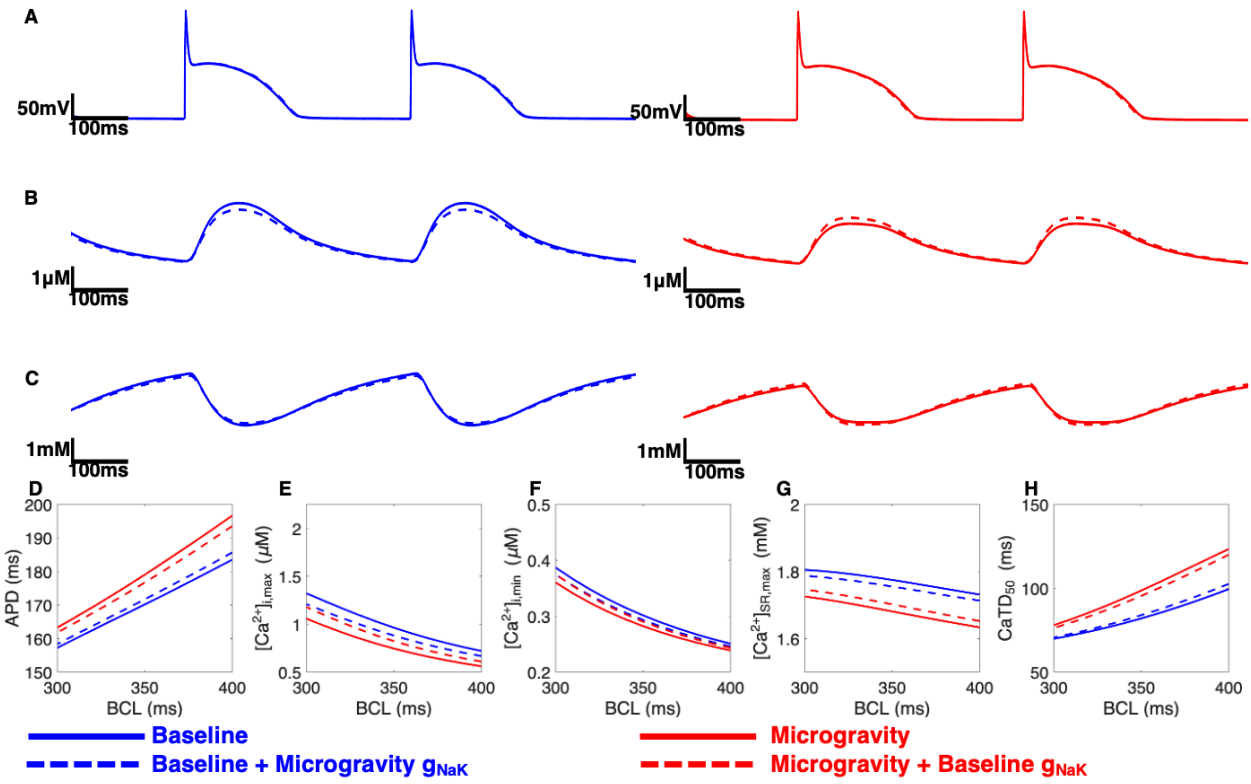

Figure 8: **Na^+/K^+ pump remodeling effects**. Action potential **(A)**, Ca^{2+} transient **(B)**, and non-junctional SR Ca^{2+} content **(C)** waveforms are analyzed at 2.5Hz with and without a g_{NaK} increase of 3.5%. The key biomarker analysis **(D-H)** shows a mixed g_{NaK} effect for the biomarkers over the BCL range of 300-400 ms.

7.3 Microgravity Remodeling Promotes Alternans by Exacerbating Ca^{2+} Handling Instabilities

The microgravity model exhibited a significantly higher threshold BCL for AP (263 ms vs 239 ms; Figure 9A) and Ca^{2+} transient alternans (277 ms vs 243 ms; Figure 9B). To evaluate the ionic underpinning of this increased alternans risk, the threshold for alternans was obtained for twelve model variations by analyzing their respective bifurcation diagrams (see Sections 6.4.4 and 6.4.6). These models were created by adding microgravity parameters to the baseline model **(10A-B)** or by removing these changes from the microgravity model **(10C-D)**. The

analysis (Figure 10A-D) reveals that the g_{RyR} and g_{LTCC} parameter remodeling allows alternans to emerge at slower pacing frequencies. In contrast, changing g_{NaK} and Kmf_{SERCA} had a mildly protective effect because changing these parameters can increase the pacing frequency required for alternans initiation. Remodeling v_{th} has a more complex, and potentially biphasic, effect on alternans susceptibility because it can lower the frequency at which alternans appears if it is added to the baseline model or removed from the microgravity model.

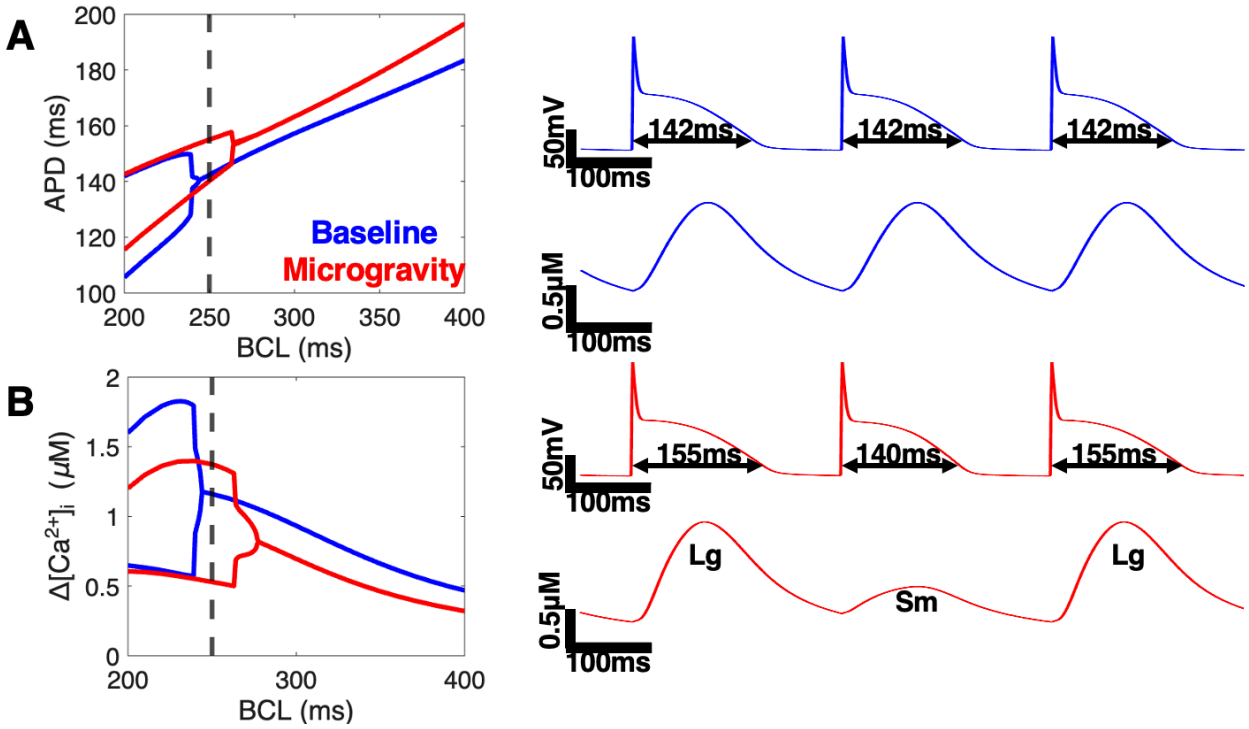

Figure 9: **Alternans risk is increased through microgravity-induced model changes**. The frequency-dependence of action potential duration **(A)** and Ca^{2+} transient amplitude **(B)** shows a higher threshold BCL for alternans initiation in the microgravity model which we interpret as a greater propensity to cardiac alternans. Representative traces of the action potential and calcium transient are shown for 4Hz pacing (dashed lines in **A-B**).

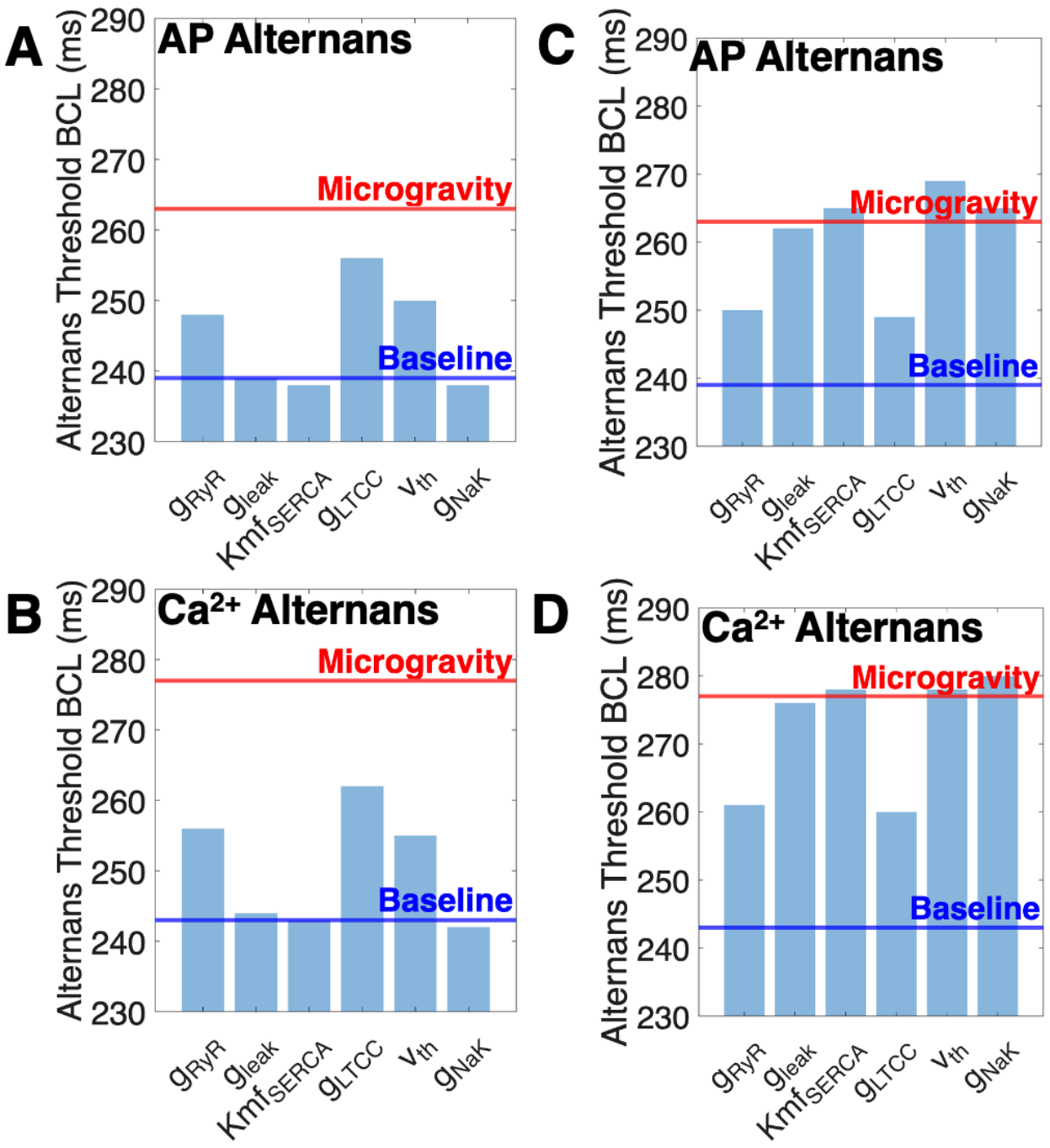

Figure 10: **Alternans risk assessment for microgravity-induced model changes**. The contributions of individual parameters to alternans risk are considered by adding microgravity parameters to the baseline model **(A-B)** or by removing these changes from the microgravity model **(C-D)**.

The conclusions of this perturbation analysis are generalized for the baseline model using the established population of models technique (Figure 11) (Morotti et al., 2017, 2021*b*; Ding et al., 2022; Morotti & Grandi, 2024). The results indicate that upregulating the RyR and reducing the LTCC conductance can increase alternans risk. The protective effect of PLB phosphorylation ($\downarrow Kmf_{SERCA}$), and in the case of AP alternans Na^+/K^+ upregulation, is also supported by the population of models analysis. Decreasing the voltage-dependent activation parameter (v_{th}) appears to correlate with increased alternans risk, as seen in its baseline model perturbation analysis; however, the microgravity-induced change in v_{th} extends beyond the variation in the population of models, making the existence of a more complex behavior feasible.

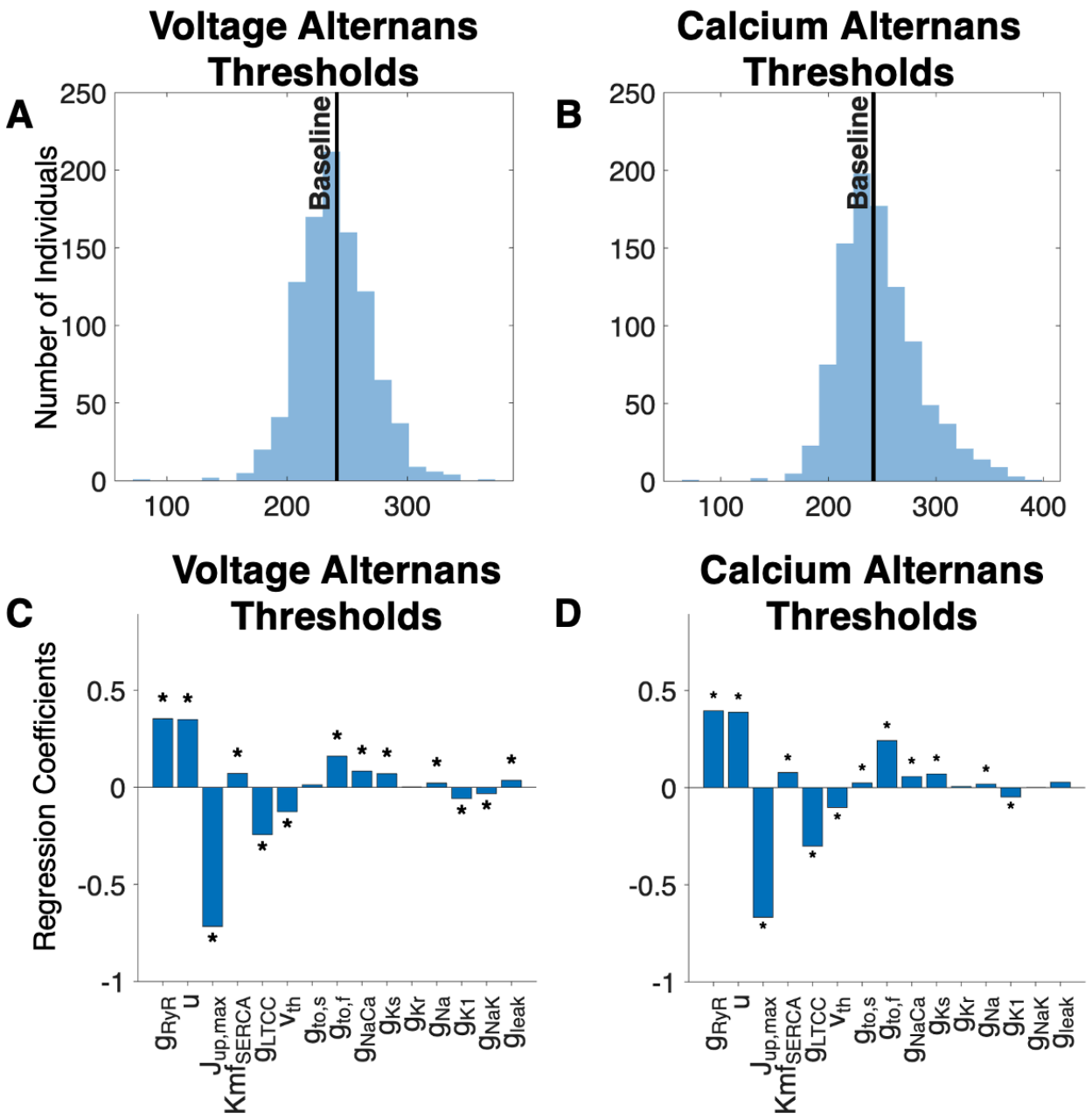

Figure 11: **Population of models analysis for cardiac alternans thresholds**. The distributions of alternans thresholds are included for both voltage **(A)** and Ca^{2+} alternans **(B)**. The alternans thresholds are correlated with the model perturbations using a partial least squares algorithm **(C-D)** (Morotti et al., 2017, 2021*b*; Ding et al., 2022; Morotti & Grandi, 2024). *p<0.05

The Mahajan Model allows alternans to be generated through either an APD restitution mechanism or a Ca^{2+} handling instability mechanism (Mahajan et al., 2008). The APD restitution mechanism is unlikely to be the primary cause of the increased alternans risk because alternans appears at a shallower APD restitution slope for the microgravity model (slope = 0.34) than the baseline model (slope = 0.60) (Figure 12A) (Echebarria & Karma, 2007; Mahajan et al., 2008).

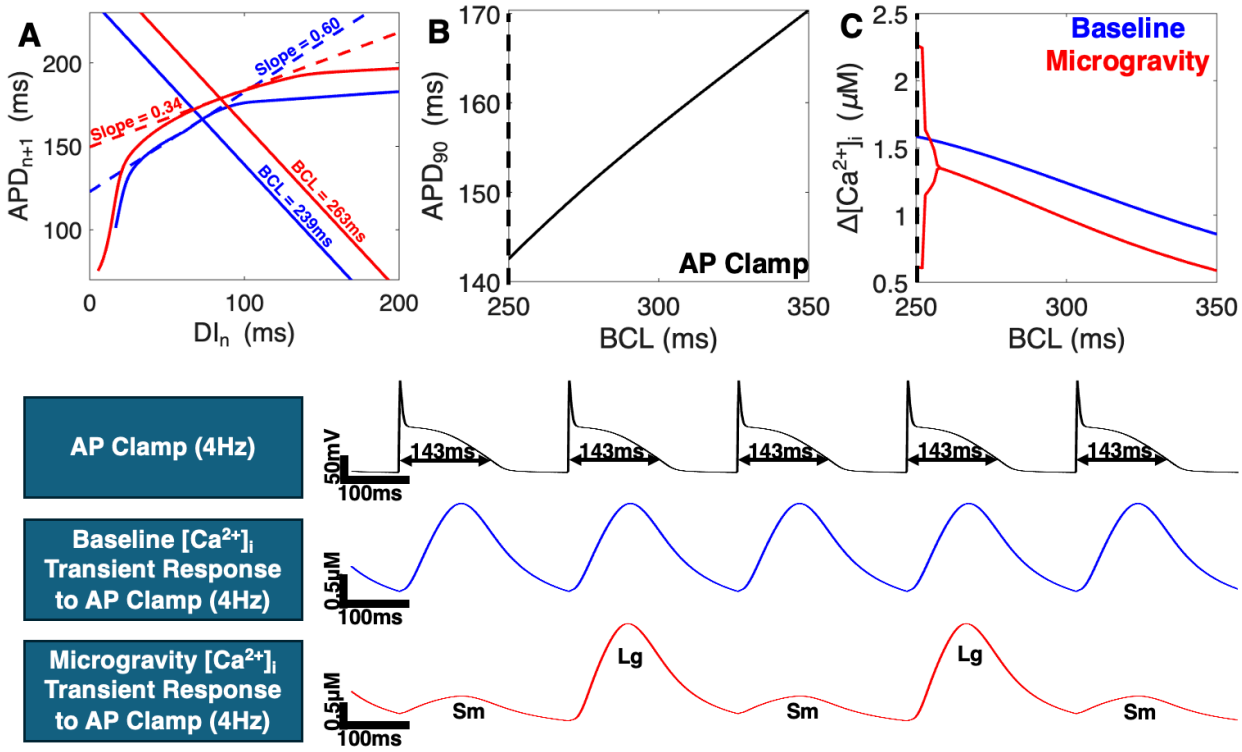

Figure 12: **Determining the mechanism of increased alternans risk**. Microgravity remodeling increases alternans risk by increasing Ca^{2+} handling instabilities. The APD restitution curves are compared for the baseline and microgravity models **(A)**. An AP clamp is applied to eliminate action potential alternans **(B)**, and Ca^{2+} alternans is still observed in the microgravity model **(C)**. The traces correspond to the AP clamp analysis when pacing at a 4Hz frequency (dashed lines in **B-C**).

To test the hypothesis that Ca^{2+} handling instabilities are the cause of increased alternans risk, we used baseline model AP recordings to control the cell membrane potential in both

models. This protocol rules out any voltage-dependent effects that may affect Ca^{2+} alternans, allowing us to isolate the Ca^{2+} handling instability effects. Under AP clamp conditions, Ca^{2+} alternans persisted in the microgravity model despite the absence of APD alternans (Figure 12B-C). As such, we conclude that the microgravity-induced changes increase alternans risk by destabilizing the Ca^{2+} cycling in the cell. Because the Mahajan Model includes the coupling of AP and Ca^{2+} transient through the NCX, Ca^{2+} alternans can in turn drive AP alternans under unclamped conditions (Mahajan et al., 2008). As such, Ca^{2+} handling instabilities account, at least in part, for the increased risk of both AP and Ca^{2+} transient alternans.

8. Discussion

8.1 Summary:

In this study, we developed and validated an *in-silico* model of ventricular cardiomyocytes that were subjected to the hindlimb unloading model of microgravity. The microgravity phenotype is associated with prolonged APD and $CaTD_{50}$ intervals and depressed cytosolic and SR Ca^{2+} concentrations. Both models exhibited APD and CaT alternans as the pacing frequency was increased, and a lower frequency was required to induce alternans in the microgravity model than the baseline model, indicating that microgravity remodeling leads to a greater vulnerability to alternans (Figure 9).

To examine the causes of this increased propensity towards cardiac alternans, we first compared APD restitution curves, which are established tools for evaluating alternans susceptibility, with steeper slopes predicting greater risk (Weiss et al., 2006). The slope of the restitution curve is shallower at the threshold for alternans initiation in the microgravity model than in the baseline model (Figure 12A), suggesting that APD restitution is not the likely mechanism of increased alternans risk. When we clamped the AP (Figure 12B-C), Ca^{2+} alternans vulnerability is enhanced in the microgravity model, even in the absence of APD alternans. This indicates that microgravity remodeling increases alternans risk through increased Ca^{2+} handling instabilities. Our analysis (Figures 10-11) revealed key roles for RyR and LTCC in mediating these effects.

8.2 Microgravity-Induced Enhancement of Alternans is Supported by Experimental Studies

The increase in threshold BCL for cardiac alternans predicted by the microgravity model is consistent with HDBR data. Grenon et al. (2005) reported an increased risk of cardiac alternans after 9-16 days of HDBR and three hours of recovery between the end of HDBR and

the bicycle stress test. Martín-Yebra et al. (2013) reported an increased risk of cardiac alternans after 5 days of HDBR in one of the two studied cohorts (5-6 hours of recovery) but not the other (26 hours of recovery). Similarly, Martín-Yebra et al. (2015) reported no change in alternans vulnerability either after 5 days of HDBR (6 hours of recovery) or 21 days of HDBR (26 hours of recovery). These results indicate that HDBR may transiently lower the threshold heart rate for alternans initiation (Martín-Yebra et al., 2015), consistent with our simulations in which alternans develops at slower pacing rates than in the baseline model.

8.3 Ionic Underpinnings of Alternans Susceptibility

In our simulations, CaMKII-mediated enhancement of RyR activity increases the threshold BCL for alternans, indicating that alternans develops at slower pacing rates. Experimental studies report divergent effects of RyR modulation on alternans. Díaz et al. (2002) induced alternans in rat cardiomyocytes by partially inhibiting RyR with tetracaine (Bers, 2001; Díaz et al., 2002), consistent with the relationship predicted by the Herrera et al. model (Herrera et al., 2023). In contrast, other studies report the opposite effect: inhibition of RyR with ryanodine suppresses alternans (Bers, 2001; Xie et al., 2008; Hinata et al., 2024), while pharmacological upregulation of RyR activity with doxorubicin promotes alternans (Bers, 2001; Azam et al., 2021). This suggests that the relationship between RyR activity and alternans susceptibility is complex and may depend on the degree and mechanism of RyR modulation, highlighting the need for further work to reconcile computational and experimental observations.

Our results show that reducing the conductance of the LTCC increases the risk of cardiac alternans, like in Herrera et al. (2023), as does negatively shifting the LTCC activation voltage dependence. In experiments, Hinata et al. (2024) shows that inhibiting the LTCC with verapamil counteracts alternans and Xie et al. (2008) shows that stimulating the LTCC with BayK8644

exacerbates alternans (Bers, 2001; Xie et al., 2008; Hinata et al., 2024). Interestingly, BayK8644 shifts activation to more negative potentials and increases channel open probability (McDonald et al., 1994). Given that the former effect is associated with alternans risk in our analysis, it is conceivable that increased LTCC availability at lower voltages, as produced by a negative activation shift, could promote alternans even when overall conductance is reduced. The discrepancy between model prediction and experimental findings may be due to differences in baseline Ca^{2+} loading states in the model versus experimental preparations. The increased vulnerability to alternans after restoring the activation shift in the microgravity model (Figure 10C-D) is consistent with this hypothesis as it presents a scenario were profound remodeling of the Ca^{2+} handling system reverses the cell response to LTCC activation shift changes.

8.4 Implications of the Findings

Our simulations show that microgravity-induced remodeling may increase susceptibility to cardiac alternans at the single-cell level. This finding is clinically relevant as cardiac alternans is an established precursors to ventricular tachycardia, ventricular fibrillation, and sudden cardiac death (Swerdlow et al., 2008; Qu & Weiss, 2023). In addition, given that microgravity is associated with pathologies such as anemia, orthostatic intolerance, and cardiac atrophy (Sy et al., 2023), an increased propensity for electrical instability could further increase the risks from microgravity-induced cardiovascular remodeling. Models like the one we developed, capable of integrating microgravity-induced remodeling, are important tools to improve arrhythmia risk assessment and support the development of pharmacological countermeasures for astronaut health.

8.5 Future Directions

Several additional forms of microgravity-induced remodeling were not included in this study and warrant further investigation in future studies.

1. Some studies suggest remodeling of the troponin complex with microgravity. Feger et al. (2016) notes an elevated protein expression of troponin T and no change in Troponin I after 5 days of *in vitro* simulated microgravity. Mair et al. (2024) shows a downregulation of the Troponin I gene after 30 days of cell culture in space. Schwoerer et al. (2008b) show a reduction in the protein expression and phosphorylation of troponin I after 2 weeks of HHT. Wnorowski et al. (2019) shows increased gene expression of troponin T and troponin I1, with no change for troponin C, after 5.5 weeks of cell culture in space. Although these findings do not reveal a consistent pattern, they suggest that microgravity may alter troponin composition and regulation, which may influence alternans risk through Ca^{2+} buffering and alterations in electromechanical activity.
2. There is some evidence of ion channel remodeling beyond what is included in this parametrization. Bilichenko et al. (2025) show a reduction in Kir6.1 (ATP-sensitive K^+ channel) and Kv1.5 (ultra-rapid K^+ channel) gene expression after 14 days of HU, and Mair et al. (2024) shows an upregulation of the KCNJ12 (inward rectifier K^+ channel) gene after 30 days of true spaceflight. These data suggest that microgravity may induce broader and more complex electrophysiological remodeling than currently captured in the model.
3. Some effects of microgravity may only emerge at the level of contraction or tissue structure. For example, Moffit et al. (2013) show increased connexin 43 protein expression after 10-14 days of HU, and Bilichenko et al. (2025) show remodeling of

stretch activated ion channels. Therefore, limiting the analysis to single-cell electrophysiology and calcium handling may overlook important contributions from mechanoelectrical coupling or tissue-level conduction dynamics.

4. Finally, this study focused on baseline conditions and did not examine ß-adrenergic stimulation. This is an important limitation because HDBR has been associated with enhanced sympathetic activity (Grenon et al., 2005; Sy et al., 2023), and microgravity has been shown to alter cellular responses to isoproterenol (Yin et al., 2008; Cui et al., 2010; Yue et al., 2015). Future work should focus on determining how microgravity-induced remodeling changes alternans risk in the presence of ß-adrenergic stimulation.

8.6 Limitations

Several limitations should be considered when interpreting the results of this study, particularly those related to assumptions used in model parametrization. The model assumes that the effects of microgravity-induced remodeling are independent of important physiological determinants of cardiac electrophysiology, such as microgravity simulation duration (Pamnani et al., 1996), species (Bartos et al., 2015), and pacing frequency (Soltis & Saucerman, 2010; Romero et al., 2011). To attenuate the limitations regarding simulation duration, we excluded studies that only considered two days of microgravity remodeling (Liu et al., 2020; Acharya et al., 2022) and note that the HU data in the model parametrization involved at least one week of microgravity simulation. We selected the longest exposure duration (1 week) for the Na^+/K^+ pump activity data to ignore transient effects (Pamnani et al., 1996).

The HU model has been iteratively designed and validated to represent microgravity-induced remodeling in rats, with contributions from many research groups (Morey-Holton & Globus, 2002), but methodological variations across studies may influence results

(Morey-Holton & Globus, 2002; Chowdhury et al., 2013). In addition, the model was originally developed for rats, and adaptations for mice introduce further variability (Morey-Holton & Globus, 2002). Integrating data from different HU implementations and species represents a limitation of this study, and differences between HU and true microgravity may also affect the accuracy of the modeled remodeling effects.

The data presented in the parametrization and validation sections (see Sections 6.2 and 7.1) was subjected to a screening protocol to prioritize strong data. This screening only accepted Western Blott data that included a quantification of error. In addition, the included *in vivo* data needed to provide evidence of biological replicates, and the included *in vitro* data needed to provide evidence of technical replicates. Schwoerer et al. (2008a) and Ibrahim et al. (2010) are examples of sources that were not considered because they did not report the number of rats that were used for any of the relevant parameters. Respress et al. (2014) is an example source that did not fully quantify the error in each Western Blott; therefore, we were unable to compare the impact of HU on RyR protein expression in this study.

The predicted depression of the Ca^{2+} transient in the model is poorly supported by the scientific literature. Both the peak systolic and end diastolic Ca^{2+} concentrations in the cytosol were highly sensitive to the LTCC conductance, which was reduced (14.8%) to match the experimentally reported effects on LTCC current. If the mechanism underlying the reduction in current is more complex than represented here, this may explain the discrepancy with experimental observations. For example, Yue et al. (2015) reported that microgravity remodeling accelerates the LTCC recovery from inactivation at -40mV membrane potentials by 11%, which would tend to increase LTCC availability. This finding suggests that LTCC regulation in

microgravity may involve a more complex mechanism that is not fully captured by the simplified representation used in the present model.

The main source of data for the microgravity model was based on primary findings in the scientific literature; however, multiple sources included comprehensive genomic or proteomic analyses (Feger et al., 2016; Wnorowski et al., 2019; Han et al., 2024*b*). Although these data are less definitive than direct functional measurements, incorporating them in future model iterations could help refine parameter estimates and improve the model predictive capability. Future work should also incorporate resources such as the NASA Open Science Data Repository (Berrios et al., 2021), to capture relevant datasets that may not appear in conventional literature searches.

8.6 Conclusion

In this study, we present a novel computational model of ventricular cardiomyocytes under microgravity conditions. Our simulations indicate that microgravity remodeling increases the risk of cardiac alternans. This heightened arrhythmogenic vulnerability is driven primarily by calcium handling instabilities. This computational framework provides critical mechanistic insight and establishes a foundation to better understand the arrhythmogenic effects of spaceflight.

9. References

Acharya, A., Nemade, H., Papadopoulos, S., Hescheler, J., Neumaier, F., Schneider, T., Rajendra Prasad, K., Khan, K., Hemmersbach, R., Gusmao, E.G., Mizi, A., Papantonis, A., & Sachinidis, A. (2022). Microgravity-induced stress mechanisms in human stem cell-derived cardiomyocytes. *iScience*, **25**(7), 104577. https://doi.org/10.1016/j.isci.2022.104577.

Anzai, T., Frey, M.A., & Nogami, A. (2014). Cardiac arrhythmias during long-duration spaceflights. *J Arrhythm*, **30**(3), 139–149. https://doi.org/10.1016/j.joa.2013.07.009.

Azam, M.A., Chakraborty, P., Bokhari, M.M., Dadson, K., Du, B., Massé, S., Si, D., Niri, A., Aggarwal, A.K., Lai, P.F.H., Riazi, S., Billia, F., & Nanthakumar, K. (2021). Cardioprotective effects of dantrolene in doxorubicin-induced cardiomyopathy in mice. *Heart Rhythm O2*, **2**(6Part B), 733–741. https://doi.org/10.1016/j.hroo.2021.08.008.

Bartos, D.C., Grandi, E., & Ripplinger, C.M. (2015). Ion channels in the heart. *Compr Physiol*, **5**(3), 1423–1464. https://doi.org/10.1002/j.2040-4603.2015.tb00647.x.

Berrios, D.C., Galazka, J., Grigorev, K., Gebre, S., & Costes, S.V. (2021). NASA GeneLab: interfaces for the exploration of space omics data. *Nucleic Acids Res*, **49**(D1), D1515–D1522. https://doi.org/10.1093/nar/gkaa887.

Bers, D.M. (2001). *Excitation-Contraction Coupling and Cardiac Contractile Force*. Springer Netherlands, Dordrecht.

Bilichenko, A.S., Zolotareva, A.D., Kamkina, O.V., Zolotarev, V.I., Rodina, A.S., Kazansky, V.E., Mitrokhin, V.M., Mladenov, M.I., & Kamkin, A.G. (2025). Simulated microgravity attenuates stretch sensitivity of mechanically gated channels in rat ventricular myocytes. *Int J Mol Sci*,; DOI: 10.3390/ijms26146653.

Chang, H., Zhang, L., Xu, P.-T., Li, Q., Sheng, J.-J., Wang, Y.-Y., Chen, Y., Zhang, L.-N., & Yu, Z.-B. (2011). Nuclear translocation of calpain-2 regulates propensity toward apoptosis in cardiomyocytes of tail-suspended rats. *J Cell Biochem*, **112**(2), 571–580. https://doi.org/10.1002/jcb.22947.

Chowdhury, P., Long, A., Harris, G., Soulsby, M.E., & Dobretsov, M. (2013). Animal model of simulated microgravity: a comparative study of hindlimb unloading via tail versus pelvic suspension. *Physiol Rep*, **1**(1), e00012. https://doi.org/10.1002/phy2.12.

Cui, Y., Zhang, S.-M., Zhang, Q.-Y., Fan, R., Li, J., Guo, H.-T., Bi, H., Wang, Y.-M., Hu, Y.-Z., Zheng, Q.-J., Gu, C.-H., Yu, S.-Q., Yi, D.-H., Li, Z.-C., & Pei, J.-M. (2010). Modulation of intracellular calcium transient in response to beta-adrenoceptor stimulation in the hearts of 4-wk-old rats during simulated weightlessness. *J Appl Physiol*, **108**(4), 838–844. https://doi.org/10.1152/japplphysiol.01055.2009.

Díaz, M.E., Eisner, D.A., & O'Neill, S.C. (2002). Depressed ryanodine receptor activity increases variability and duration of the systolic Ca2+ transient in rat ventricular myocytes. *Circ Res*, **91**(7), 585–593. https://doi.org/10.1161/01.res.0000035527.53514.c2.

Ding, Y., Lang, D., Yan, J., Bu, H., Li, H., Jiao, K., Yang, J., Ni, H., Morotti, S., Le, T., Clark, K.J., Port, J., Ekker, S.C., Cao, H., Zhang, Y., Wang, J., Grandi, E., Li, Z., Shi, Y., … Xu, X. (2022). A phenotype-based forward genetic screen identifies Dnajb6 as a sick sinus syndrome gene. *eLife*,; DOI: 10.7554/eLife.77327.

Echebarria, B. & Karma, A. (2007). Mechanisms for initiation of cardiac discordant alternans. *Eur Phys J Spec Top*, **146**(1), 217–231. https://doi.org/10.1140/epjst/e2007-00182-y.

Feger, B.J., Thompson, J.W., Dubois, L.G., Kommaddi, R.P., Foster, M.W., Mishra, R., Shenoy, S.K., Shibata, Y., Kidane, Y.H., Moseley, M.A., Carnell, L.S., & Bowles, D.E. (2016).

Microgravity induces proteomics changes involved in endoplasmic reticulum stress and mitochondrial protection. *Sci Rep*, **6**, 34091. https://doi.org/10.1038/srep34091.

Forghani, P., Liu, W., Wang, Z., Ling, Z., Takaesu, F., Yang, E., Tharp, G.K., Nielsen, S., Doraisingam, S., Countryman, S., Davis, M.E., Wu, R., Jia, S., & Xu, C. (2025). Spaceflight alters protein levels and gene expression associated with stress response and metabolic characteristics in human cardiac spheroids. *Biomaterials*, **317**, 123080. https://doi.org/10.1016/j.biomaterials.2024.123080.

Grenon, S.M., Xiao, X., Hurwitz, S., Ramsdell, C.D., Sheynberg, N., Kim, C., Williams, G.H., & Cohen, R.J. (2005). Simulated microgravity induces microvolt T wave alternans. *Ann Noninvasive Electrocardiol*, **10**(3), 363–370. https://doi.org/10.1111/j.1542-474X.2005.00654.x.

Guarnieri, S., Morabito, C., Bevere, M., Lanuti, P., & Mariggiò, M.A. (2021). A protective strategy to counteract the oxidative stress induced by simulated microgravity on H9C2 cardiomyocytes. *Oxid Med Cell Longev*, **2021**, 9951113. https://doi.org/10.1155/2021/9951113.

Halet, G., Viard, P., Morel, J.L., Mironneau, J., & Mironneau, C. (1999). Effects of hindlimb suspension on cytosolic Ca2+ and [3H]ryanodine binding in cardiac myocytes. *Am J Physiol*, **276**(4), H1131-6. https://doi.org/10.1152/ajpheart.1999.276.4.H1131.

Han, H., Jia, H., Wang, Y.-F., & Song, J.-P. (2024*a*). Cardiovascular adaptations and pathological changes induced by spaceflight: from cellular mechanisms to organ-level impacts. *Mil Med Res*, **11**(1), 68. https://doi.org/10.1186/s40779-024-00570-3.

Han, X., Qu, L., Yu, M., Ye, L., Shi, L., Ye, G., Yang, J., Wang, Y., Fan, H., Wang, Y., Tan, Y., Wang, C., Li, Q., Lei, W., Chen, J., Liu, Z., Shen, Z., Li, Y., & Hu, S. (2024*b*). Thiamine-modified metabolic reprogramming of human pluripotent stem cell-derived cardiomyocyte under space microgravity. *Signal Transduct Target Ther*, **9**(1), 86. https://doi.org/10.1038/s41392-024-01791-7.

Heijman, J., Erfanian Abdoust, P., Voigt, N., Nattel, S., & Dobrev, D. (2016). Computational models of atrial cellular electrophysiology and calcium handling, and their role in atrial fibrillation. *J Physiol (Lond)*, **594**(3), 537–553. https://doi.org/10.1113/JP271404.

Herrera, N.T., Zhang, X., Ni, H., Maleckar, M.M., Heijman, J., Dobrev, D., Grandi, E., & Morotti, S. (2023). Dual effects of the small-conductance Ca2+-activated K+ current on human atrial electrophysiology and Ca2+-driven arrhythmogenesis: an in silico study. *Am J Physiol Heart Circ Physiol*, **325**(4), H896–H908. https://doi.org/10.1152/ajpheart.00362.2023.

Hinata, Y., Sasaki, D., Matsuura, K., & Shimizu, T. (2024). Induction of cardiac alternans in human iPS-derived cardiomyocytes through β-adrenergic receptor stimulation. *Physiol Rep*, **12**(24), e70152. https://doi.org/10.14814/phy2.70152.

Ibrahim, M., Al Masri, A., Navaratnarajah, M., Siedlecka, U., Soppa, G.K., Moshkov, A., Al-Saud, S.A., Gorelik, J., Yacoub, M.H., & Terracciano, C.M.N. (2010). Prolonged mechanical unloading affects cardiomyocyte excitation-contraction coupling, transverse-tubule structure, and the cell surface. *FASEB J*, **24**(9), 3321–3329. https://doi.org/10.1096/fj.10-156638.

Ibrahim, M., Kukadia, P., Siedlecka, U., Cartledge, J.E., Navaratnarajah, M., Tokar, S., Van Doorn, C., Tsang, V.T., Gorelik, J., Yacoub, M.H., & Terracciano, C.M. (2012). Cardiomyocyte Ca2+ handling and structure is regulated by degree and duration of mechanical load variation. *J Cell Mol Med*, **16**(12), 2910–2918. https://doi.org/10.1111/j.1582-4934.2012.01611.x.

Ito, K., Nakayama, M., Hasan, F., Yan, X., Schneider, M.D., & Lorell, B.H. (2003). Contractile reserve and calcium regulation are depressed in myocytes from chronically unloaded hearts. *Circulation*, **107**(8), 1176–1182. https://doi.org/10.1161/01.cir.0000051463.72137.96.

Liu, C., Zhong, G., Zhou, Y., Yang, Y., Tan, Y., Li, Y., Gao, X., Sun, W., Li, J., Jin, X., Cao, D., Yuan, X., Liu, Z., Liang, S., Li, Y., Du, R., Zhao, Y., Xue, J., Zhao, D., … Li, Y. (2020). Alteration of calcium signalling in cardiomyocyte induced by simulated microgravity and hypergravity. *Cell Prolif*, **53**(3), e12783. https://doi.org/10.1111/cpr.12783.

Mahajan, A., Shiferaw, Y., Sato, D., Baher, A., Olcese, R., Xie, L.-H., Yang, M.-J., Chen, P.-S., Restrepo, J.G., Karma, A., Garfinkel, A., Qu, Z., & Weiss, J.N. (2008). A rabbit ventricular action potential model replicating cardiac dynamics at rapid heart rates. *Biophys J*, **94**(2), 392–410. https://doi.org/10.1529/biophysj.106.98160.

Mair, D.B., Tsui, J.H., Higashi, T., Koenig, P., Dong, Z., Chen, J.F., Meir, J.U., Smith, A.S.T., Lee, P.H.U., Ahn, E.H., Countryman, S., Sniadecki, N.J., & Kim, D.-H. (2024). Spaceflight-induced contractile and mitochondrial dysfunction in an automated heart-on-a-chip platform. *Proc Natl Acad Sci USA*, **121**(40), e2404644121. https://doi.org/10.1073/pnas.2404644121.

Martín-Yebra, A., Caiani, E.G., Monasterio, V., Pellegrini, A., Laguna, P., & Martínez, J.P. (2015). Evaluation of T-wave alternans activity under stress conditions after 5 d and 21 d of sedentary head-down bed rest. *Physiol Meas*, **36**(10), 2041–2055. https://doi.org/10.1088/0967-3334/36/10/2041.

Martín-Yebra, A., Monasterie, V., Pellegrini, A., Laguna, P., Caiani, E., & Martinez, J.P. (2013). Effect of simulated microgravity by head-down bed rest on T wave alternans. *IEEE*,.

Martín-Yebra, A., Monasterio, V., Laguna, P., Mart□nez, J.P., & Caiani, E. (2017). Evaluation of Changes in T-wave Alternans Induced by 60 Days of Immobilization by Head-down Bed-rest. In *2017 Computing in Cardiology Conference (CinC)*. Computing in Cardiology.

Martín-Yebra, A., Monasterio, V., Landreani, F., Laguna, P., Pablo Martínez, J., & Caiani, E.G. (2019). Assessment of ventricular repolarization instability in terms of T-wave alternans induced by head-down bed-rest immobilization. *Physiol Meas*, **40**(10), 104001. https://doi.org/10.1088/1361-6579/ab4c18.

Mathews, W.R., DuCharme, D.W., Hamlyn, J.M., Harris, D.W., Mandel, F., Clark, M.A., & Ludens, J.H. (1991). Mass spectral characterization of an endogenous digitalislike factor from human plasma. *Hypertension*, **17**(6 Pt 2), 930–935. https://doi.org/10.1161/01.hyp.17.6.930.

McDonald, T.F., Pelzer, S., Trautwein, W., & Pelzer, D.J. (1994). Regulation and modulation of calcium channels in cardiac, skeletal, and smooth muscle cells. *Physiol Rev*, **74**(2), 365–507. https://doi.org/10.1152/physrev.1994.74.2.365.

Moffitt, J.A., Henry, M.K., Welliver, K.C., Jepson, A.J., & Garnett, E.R. (2013). Hindlimb unloading results in increased predisposition to cardiac arrhythmias and alters left ventricular connexin 43 expression. *Am J Physiol Regul Integr Comp Physiol*, **304**(5), R362-73. https://doi.org/10.1152/ajpregu.00391.2012.

Møller, B., Vaag, A., & Johansen, T. (1990). Ouabain inhibition of the sodium-potassium pump: estimation of ED50 in different types of human leucocytes in vitro. *Br J Clin Pharmacol*, **29**(1), 93–100. https://doi.org/10.1111/j.1365-2125.1990.tb03607.x.

Morey-Holton, E.R. & Globus, R.K. (2002). Hindlimb unloading rodent model: technical aspects. *J Appl Physiol*, **92**(4), 1367–1377. https://doi.org/10.1152/japplphysiol.00969.2001.

Morotti, S. & Grandi, E. (2024). Population-Based Computational Approaches to Investigate Cardiac Arrhythmia Risk. In *Molecular and computational modeling of cardiac function*, ed.

Jue T, Handbook of modern biophysics, pp. 181–198. Springer Nature Switzerland, Cham. https://doi.org/10.1007/978-3-031-73730-5_5.

Morotti, S., Liu, C., Hegyi, B., Ni, H., Fogli Iseppe, A., Wang, L., Pritoni, M., Ripplinger, C.M., Bers, D.M., Edwards, A.G., & Grandi, E. (2021*a*). Quantitative cross-species translators of cardiac myocyte electrophysiology: Model training, experimental validation, and applications. *Sci Adv*, **7**(47), eabg0927. https://doi.org/10.1126/sciadv.abg0927.

Morotti, S., Ni, H., Peters, C.H., Rickert, C., Asgari-Targhi, A., Sato, D., Glukhov, A.V., Proenza, C., & Grandi, E. (2021*b*). Intracellular na+ modulates pacemaking activity in murine sinoatrial node myocytes: an in silico analysis. *Int J Mol Sci*,; DOI: 10.3390/ijms22115645.

Morotti, S., Nieves-Cintrón, M., Nystoriak, M.A., Navedo, M.F., & Grandi, E. (2017). Predominant contribution of L-type Cav1.2 channel stimulation to impaired intracellular calcium and cerebral artery vasoconstriction in diabetic hyperglycemia. *Channels (Austin)*, **11**(4), 340–346. https://doi.org/10.1080/19336950.2017.1293220.

Odermatt, A., Kurzydlowski, K., & MacLennan, D.H. (1996). The vmax of the Ca2+-ATPase of cardiac sarcoplasmic reticulum (SERCA2a) is not altered by Ca2+/calmodulin-dependent phosphorylation or by interaction with phospholamban. *J Biol Chem*, **271**(24), 14206–14213. https://doi.org/10.1074/jbc.271.24.14206.

van Oort, R.J., McCauley, M.D., Dixit, S.S., Pereira, L., Yang, Y., Respress, J.L., Wang, Q., De Almeida, A.C., Skapura, D.G., Anderson, M.E., Bers, D.M., & Wehrens, X.H.T. (2010). Ryanodine receptor phosphorylation by calcium/calmodulin-dependent protein kinase II promotes life-threatening ventricular arrhythmias in mice with heart failure. *Circulation*, **122**(25), 2669–2679. https://doi.org/10.1161/CIRCULATIONAHA.110.982298.

Pamnani, M.B., Mo, Z., Chen, S., Bryant, H.J., White, R.J., & Haddy, F.J. (1996). Effects of head down tilt on hemodynamics, fluid volumes, and plasma Na-K pump inhibitor in rats. *Aviat Space Environ Med*, **67**(10), 928–934.

Pavy-Le Traon, A., Heer, M., Narici, M.V., Rittweger, J., & Vernikos, J. (2007). From space to Earth: advances in human physiology from 20 years of bed rest studies (1986-2006). *Eur J Appl Physiol*, **101**(2), 143–194. https://doi.org/10.1007/s00421-007-0474-z.

Qu, Z. & Weiss, J.N. (2023). Cardiac alternans: from bedside to bench and back. *Circ Res*, **132**(1), 127–149. https://doi.org/10.1161/CIRCRESAHA.122.321668.

Respress, J.L., Gershovich, P.M., Wang, T., Reynolds, J.O., Skapura, D.G., Sutton, J.P., Miyake, C.Y., & Wehrens, X.H.T. (2014). Long-term simulated microgravity causes cardiac RyR2 phosphorylation and arrhythmias in mice. *Int J Cardiol*, **176**(3), 994–1000. https://doi.org/10.1016/j.ijcard.2014.08.138.

Ritter, M., Su, Z., Xu, S., Shelby, J., & Barry, W.H. (2000). Cardiac unloading alters contractility and calcium homeostasis in ventricular myocytes. *J Mol Cell Cardiol*, **32**(4), 577–584. https://doi.org/10.1006/jmcc.2000.1101.

Rojo-García, A.V., Vanmunster, M., Pacolet, A., & Suhr, F. (2023). Physical inactivity by tail suspension alters markers of metabolism, structure, and autophagy of the mouse heart. *Physiol Rep*, **11**(2), e15574. https://doi.org/10.14814/phy2.15574.

Romero, L., Carbonell, B., Trenor, B., Rodríguez, B., Saiz, J., & Ferrero, J.M. (2011). Systematic characterization of the ionic basis of rabbit cellular electrophysiology using two ventricular models. *Prog Biophys Mol Biol*, **107**(1), 60–73. https://doi.org/10.1016/j.pbiomolbio.2011.06.012.

Sakowski, C., Starc, V., Smith, S.M., & Schlegel, T.T. (2011). Sedentary long-duration head-down bed rest and ECG repolarization heterogeneity. *Aviat Space Environ Med*, **82**(4), 416–423. https://doi.org/10.3357/asem.2945.2011.

Schwoerer, A.P., Biermann, D., & Ehmke, H. (2024). Ventricular unloading causes prolongation of the QT interval and induces ventricular arrhythmias in rat hearts. *Front Physiol*, **15**, 1346093. https://doi.org/10.3389/fphys.2024.1346093.

Schwoerer, A.P., Melnychenko, I., Goltz, D., Hedinger, N., Broichhausen, I., El-Armouche, A., Eschenhagen, T., Volk, T., & Ehmke, H. (2008*a*). Unloaded rat hearts in vivo express a hypertrophic phenotype of cardiac repolarization. *J Mol Cell Cardiol*, **45**(5), 633–641. https://doi.org/10.1016/j.yjmcc.2008.02.271.

Schwoerer, A.P., Neef, S., Broichhausen, I., Jacubeit, J., Tiburcy, M., Wagner, M., Biermann, D., Didié, M., Vettel, C., Maier, L.S., Zimmermann, W.H., Carrier, L., Eschenhagen, T., Volk, T., El-Armouche, A., & Ehmke, H. (2013). Enhanced Ca^{2}+ influx through cardiac L-type Ca^{2}+ channels maintains the systolic Ca^{2}+ transient in early cardiac atrophy induced by mechanical unloading. *Pflugers Arch*, **465**(12), 1763–1773. https://doi.org/10.1007/s00424-013-1316-y.

Schwoerer, A.P., Neuber, C., Schmechel, A., Melnychenko, I., Mearini, G., Boknik, P., Kirchhefer, U., Schmitz, W., Ehmke, H., Eschenhagen, T., & El-Armouche, A. (2008*b*). Mechanical unloading of the rat heart involves marked changes in the protein kinase-phosphatase balance. *J Mol Cell Cardiol*, **45**(6), 846–852. https://doi.org/10.1016/j.yjmcc.2008.09.003.

Shi, J.-S., Li, D., Li, N., Lin, L., Yang, Y.-J., Tang, Y., Sun, T., Yuan, W.-J., & Ren, A.-J. (2010). Inhibition of L-type calcium currents by salusin-beta in rat cardiac ventricular myocytes. *Peptides*, **31**(6), 1146–1149. https://doi.org/10.1016/j.peptides.2010.03.016.

Solbiati, S., Landreani, F., Turcato, M., Martin-Yebra, A., Costantini, L., Vaida, P., & Caiani, E.G. (2020*a*). Analysis of changes in cardiac circadian rhythms of RR and QT induced by a 60-day head-down bed rest with and without nutritional countermeasure. *Eur J Appl Physiol*, **120**(7), 1699–1710. https://doi.org/10.1007/s00421-020-04404-7.

Solbiati, S., Martin-Yebra, A., Vaïda, P., & Caiani, E.G. (2020*b*). Evaluation of Cardiac Circadian Rhythm Deconditioning Induced by 5-to-60 Days of Head-Down Bed Rest. *Front Physiol*, **11**, 612188. https://doi.org/10.3389/fphys.2020.612188.

Soltis, A.R. & Saucerman, J.J. (2010). Synergy between CaMKII substrates and β-adrenergic signaling in regulation of cardiac myocyte Ca(2+) handling. *Biophys J*, **99**(7), 2038–2047. https://doi.org/10.1016/j.bpj.2010.08.016.

Swerdlow, C.D., Zhou, X., Voroshilovsky, O., Abeyratne, A., & Gillberg, J. (2008). High amplitude T-wave alternans precedes spontaneous ventricular tachycardia or fibrillation in ICD electrograms. *Heart Rhythm*, **5**(5), 670–676. https://doi.org/10.1016/j.hrthm.2008.02.018.

Sy, M.R., Keefe, J.A., Sutton, J.P., & Wehrens, X.H.T. (2023). Cardiac function, structural, and electrical remodeling by microgravity exposure. *Am J Physiol Heart Circ Physiol*, **324**(1), H1–H13. https://doi.org/10.1152/ajpheart.00611.2022.

Tomek, J., Zhou, X., Martinez-Navarro, H., Holmes, M., Bury, T., Berg, L.A., Tomkova, M., Jo, E., Nagy, N., Bertrand, A., Bueno-Orovio, A., Colman, M., Rodriguez, B., Bers, D., & Heijman, J. (2025). T-World: A highly general computational model of a human ventricular myocyte. *BioRxiv*,; DOI: 10.1101/2025.03.24.645031.

Trayanova, N.A., Lyon, A., Shade, J., & Heijman, J. (2024). Computational modeling of cardiac electrophysiology and arrhythmogenesis: toward clinical translation. *Physiol Rev*, **104**(3), 1265–1333. https://doi.org/10.1152/physrev.00017.2023.

United States Census Bureau (n.d.). https://www2.census.gov/programs-surveys/acs/tech_docs/accuracy/percchg.pdf. Available at: https://www2.census.gov/programs-surveys/acs/tech_docs/accuracy/percchg.pdf [Accessed February 12, 2026].

Uchinoumi, H., Yang, Y., Oda, T., Li, N., Alsina, K.M., Puglisi, J.L., Chen-Izu, Y., Cornea, R.L., Wehrens, X.H.T., & Bers, D.M. (2016). CaMKII-dependent phosphorylation of RyR2 promotes targetable pathological RyR2 conformational shift. *J Mol Cell Cardiol*, **98**, 62–72. https://doi.org/10.1016/j.yjmcc.2016.06.007.

Weiss, J.N., Karma, A., Shiferaw, Y., Chen, P.-S., Garfinkel, A., & Qu, Z. (2006). From pulsus to pulseless: the saga of cardiac alternans. *Circ Res*, **98**(10), 1244–1253. https://doi.org/10.1161/01.RES.0000224540.97431.f0.

Wnorowski, A., Sharma, A., Chen, H., Wu, H., Shao, N.-Y., Sayed, N., Liu, C., Countryman, S., Stodieck, L.S., Rubins, K.H., Wu, S.M., Lee, P.H.U., & Wu, J.C. (2019). Effects of Spaceflight on Human Induced Pluripotent Stem Cell-Derived Cardiomyocyte Structure and Function. *Stem Cell Reports*, **13**(6), 960–969. https://doi.org/10.1016/j.stemcr.2019.10.006.

Wright, P.T., Sanchez-Alonso, J.L., Lucarelli, C., Alvarez-Laviada, A., Poulet, C.E., Bello, S.O., Faggian, G., Terracciano, C.M., & Gorelik, J. (2018). Partial Mechanical Unloading of the Heart Disrupts L-Type Calcium Channel and Beta-Adrenoceptor Signaling Microdomains. *Front Physiol*, **9**, 1302. https://doi.org/10.3389/fphys.2018.01302.

Xie, L.-H., Sato, D., Garfinkel, A., Qu, Z., & Weiss, J.N. (2008). Intracellular Ca alternans: coordinated regulation by sarcoplasmic reticulum release, uptake, and leak. *Biophys J*, **95**(6), 3100–3110. https://doi.org/10.1529/biophysj.108.130955.

Yin, W., Liu, J.-C., Fan, R., Sun, X.-Q., Ma, J., Feng, N., Zhang, Q.Y., Yin, Z., Zhang, S.-M., Guo, H.-T., Bi, H., Wang, Y.-M., Sun, X., Cheng, L., Cui, Q., Yu, S.-Q., Yi, D.-H., & Pei, J.-M. (2008). Modulation of {beta}-adrenoceptor signaling in the hearts of 4-wk simulated weightlessness rats. *J Appl Physiol*, **105**(2), 569–574. https://doi.org/10.1152/japplphysiol.01381.2007.

Yue, Z.-J., Xu, P.-T., Jiao, B., Chang, H., Song, Z., Xie, M.-J., & Yu, Z.-B. (2015). Nitric Oxide Protects L-Type Calcium Channel of Cardiomyocyte during Long-Term Isoproterenol Stimulation in Tail-Suspended Rats. *Biomed Res Int*, **2015**, 780814. https://doi.org/10.1155/2015/780814.